Title

$Co_{11}Li[(OH)_5O][(PO_3OH)(PO_4)_5]$, a Lithium-Stabilized, Mixed-Valent Cobalt(II,III) Hydroxide Phosphate Framework

Journal

INORGANIC CHEMISTRY, 56(18)

ISSN

0020-1669

Authors

Ludwig, Jennifer

Gepraegs, Stephan

Nordlund, Dennis

et al.

Publication Date

2017

DOI

10.1021/acs.inorgchem.7b01152

Peer reviewed

$Co_{11}Li[(OH)_5O][(PO_3OH)(PO_4)_5]$, a Lithium-Stabilized, Mixed-Valent Cobalt (II,III) Hydroxide Phosphate Framework

Journal:	*Inorganic Chemistry*
Manuscript ID	Draft
Manuscript Type:	Article
Date Submitted by the Author:	n/a
Complete List of Authors:	Ludwig, Jennifer; Technical University of Munich, Department of Chemistry Geprägs, Stephan; Bayerische Akademie der Wissenschaften, Walther-Meißner-Institut Nordlund, Dennis; Stanford Synchrotron Radiation Lightsource, SLAC National Accelerator Laboratory Doeff, Marca; Lawrence Berkeley National Laboratory, Energy Storage and Distributed Resources Division Nilges, Tom; Technical University of Munich, Department of Chemistry

$Co_{11}Li[(OH)_5O][(PO_3OH)(PO_4)_5]$, a Lithium-Stabilized, Mixed-Valent Cobalt (II,III) Hydroxide Phosphate Framework

Jennifer Ludwig [a,*], *Stephan Geprägs* [b], *Dennis Nordlund* [c], *Marca M. Doeff* [d], *and Tom Nilges* [a,*]

[a] Technical University of Munich, Department of Chemistry, Synthesis and Characterization of Innovative Materials, Lichtenbergstr. 4, 85747 Garching, Germany

[b] Walther Meissner Institute, Bavarian Academy of Sciences and Humanities, Walther-Meissner-Str. 8, 85747 Garching, Germany

[c] Stanford Synchrotron Radiation Lightsource, SLAC National Accelerator Laboratory, 2575 Sand Hill Rd, Menlo Park, CA, 94025, USA

[d] Lawrence Berkeley National Laboratory, Energy Storage and Distributed Resources Division, 1 Cyclotron Rd, Berkeley, CA, 94720, USA

KEYWORDS. Cobalt lithium hydroxide phosphate, hydrothermal synthesis, metastable compounds, crystal structure, thermal stability

ABSTRACT. A new metastable phase, featuring a lithium-stabilized mixed-valence cobalt (II,III) hydroxide phosphate framework, $Co_{11.0(1)}Li_{1.0(2)}[(OH)_5O][(PO_3OH)(PO_4)_5]$, corresponding to the simplified composition $Co_{1.84(2)}Li_{0.16(3)}(OH)PO_4$, is prepared by hydrothermal synthesis. Because the pH-dependent formation of other phases such as $Co_3(OH)_2(PO_3OH)_2$ and olivine-type $LiCoPO_4$ competes in the process, a pH value of 5.0 is crucial for obtaining a single-phase material. The crystals with dimensions of 15 µm × 30 µm exhibit a unique elongated triangular pyramid morphology with a lamellar fine structure. Powder X-ray diffraction experiments reveal that the phase is isostructural with the natural phosphate minerals holtedahlite and satterlyite, and crystallizes in the trigonal space group $P31m$ (a = 11.2533(4) Å, c = 4.9940(2) Å, V = 547.70(3) Å^3, Z = 1). The three-dimensional network structure is characterized by partially Li-substituted, octahedral [$M_2O_8(OH)$] (M = Co, Li) dimer units which form double chains that run along the [001] direction and are connected by [PO_4] and [$PO_3(OH)$] tetrahedra. Because no Li-free $P31m$-type $Co_2(OH)PO_4$ phase could be prepared, it can be assumed that the Li ions are crucial for the stabilization of the framework. Co L-edge X-ray absorption spectroscopy demonstrates that the cobalt ions adopt the oxidation states +2 and +3 and hence, provides further evidence for the incorporation of Li in the charge-balanced framework. The presence of three independent hydroxyl groups is further confirmed by infrared spectroscopy. Magnetization measurements imply a paramagnetic to antiferromagnetic transition at T = 25 K and a spin-glass-like behavior with a blocking temperature of ~9 K. The metastable character of the phase is demonstrated by thermogravimetric analysis and differential scanning calorimetry, which above 558 °C reveal a two-step decomposition to CoO, $Co_3(PO_4)_2$, and olivine-type $LiCoPO_4$ with release of water and oxygen.

INTRODUCTION

Transition-metal phosphates offer great structural and chemical diversity, which allows for interesting physical properties and therefore opens up a great portfolio of possible applications, for example in adsorption,[1] semiconductive glasses,[2] nonlinear optics,[3] catalysis,[4-7] and batteries.[8-11] In particular iron phosphates have been the object of considerable study because of the relative abundance of iron in nature,[8, 12] whereas cobalt phosphates have been less investigated. An interesting catalyst for oxygen evolution reactions (OER) is, for example, the Co–Pi system, which contains mixed-valent Co ions in a complex hydroxide–hydrogen phosphate–phosphate environment.[5-7] Since many natural phosphates represent hydrothermal minerals, the hydrothermal synthesis technique, mimicking nature, is a powerful tool for preparing compounds isostructural with natural minerals as well as original structures[13] and hence, to further explore the class of cobalt phosphates.

The most prominent compound of this class is probably olivine-type $LiCoPO_4$ (space group: *Pnma*), which belongs to the group of lithium transition-metal orthophosphates $LiMPO_4$ (M = Fe, Mn, Co, Ni).[8] The three-dimensional network structure hosts zigzag chains of $[CoO_6]$ octahedra that run along the [001] direction and are connected by $[PO_4]$ tetrahedra, whereas the Li ions are located in channels running along the [010] and [001] directions.[8] $LiCoPO_4$ has been studied extensively in recent years because of its potential use as a high-voltage cathode material for lithium-ion batteries and high theoretical gravimetric energy density of 802 $Wh \cdot kg^{-1}$, which might bring a significant improvement to current Li-ion battery technology.[9, 10, 14-16] In addition, also the magnetic properties have been investigated in a number of studies,[17, 18] revealing a weak ferromagnetic moment in the antiferromagnetic state below the Néel temperature of T_N = 21.9 K.

Because of their interesting magnetic characteristics, the class of cobalt hydroxide phosphates has also been receiving increasing attention. The most important representative is $Co_2(OH)PO_4$, for which two polymorphs with orthorhombic (space group: *Pnnm*) and tetragonal ($I4_1/amd$) structures are known.[19, 20] The orthorhombic $Co_2(OH)PO_4$ polymorph, which adopts the adamite structure type ($Zn_2(OH)AsO_4$, space group: *Pnnm*),[21, 22] was first reported by Harrison and co-workers[19] in 1995. The three-dimensional network structure is built from chains of edge-sharing $[CoO_4(OH)_2]$ octahedra, which run along [001] and are cross-linked by dimers of edge-shared $[CoO_4(OH)]$ trigonal bipyramids and $[PO_4]$ tetrahedra. The compound was found to be the first ordered cobalt phosphate that exhibits a three-dimensional antiferromagnetic long-range order below $T = 70$ K and a spin-glass-like state with a blocking temperature of 13 K. This spin-glass-like behavior was related to a magnetic frustration of the Co^{2+} ions in the $[CoO_5]$ dimers due to the existence of antiferromagnetic interactions between the neighboring $[CoO_6]_\infty$ chains as well as a ferromagnetic interaction between the chains and the dimers.[23] In a number of studies by de Pedro and co-workers,[24-26] it was further demonstrated that the magnetic properties of adamite-type *Pnnm*-$Co_2(OH)PO_4$ can be modified by substituting Co by other magnetic transition-metal ions such as Ni, Cu, and Mn. Furthermore, also the properties of solid solutions of phosphate and arsenate, $Co_2(OH)(PO_4)_{1-x}(AsO_4)_x$ ($x = 0$–1), have been explored.[27]

The tetragonal $Co_2(OH)PO_4$ polymorph (space group: $I4_1/amd$) was recently reported by Wang *et al.*[20] The phase is isostructural with the minerals caminite $Mg_{1.33}[SO_4(OH)_{0.66}(H_2O)_{0.33}]$ ($MgSO_4 \cdot \frac{1}{3}\, Mg(OH)_2 \cdot \frac{1}{3}\, H_2O$)[28] and lipscombite $Fe_{2-y}(OH)PO_4$ ($0 \le y \le 2/3$).[29] The three-dimensional framework features chains of face-sharing $[CoO_4(OH)_2]$ octahedra, which run along the [100] and [010] directions and are connected by tri-bridging OH groups and $[PO_4]$ tetrahedra. Magnetization experiments revealed a ferromagnetic moment below 20 K, which is most likely

caused by a canted, antiferromagnetic spin structure. Furthermore, a two-step switching of the magnetization as a function of the magnetic field was found at 2 K. To explain this behavior, a spin-flip component perpendicular to the crystallographic [001] direction and a spin-flop component oriented along [001] were postulated.[20]

In this work, we report on the hydrothermal synthesis and characterization of a new trigonal, *P*31*m*-type cobalt hydroxide phosphate, which is stabilized by Li substitution and exhibits the crystal-chemical composition $Co_{11.0(1)}Li_{1.0(2)}[(OH)_5O][(PO_3OH)(PO_4)_5]$, simplified to $Co_{1.84(2)}Li_{0.16(3)}(OH)PO_4$ for better comparability with the sum formula $Co_2(OH)PO_4$ of the adamite- (*Pnnm*) and caminite-type ($I4_1/amd$) materials. The phase is isostructural with the natural phosphate minerals satterlyite[30, 31] $Fe_{9.24}Mg_{2.76}(OH,O)_6(PO_3OH)(PO_4)_5$ (found at the Big Fish River area, Yukon Territory, Canada; simplified formula: $Fe_{1.54}Mg_{0.46}(OH)PO_4$), and holtedahlite[32] $Mg_{12}(OH,O)_6(CO_3)_{0.24}(PO_3OH)_{0.76}(PO_4)_5$ (from Modum, Norway; simplified: $Mg_2(OH)(CO_3)_{0.04}(PO_4)_{0.96}$) as well as its synthetic analogue $Mg_{12}(OH,O)_6(PO_3OH)(PO_4)_5$ (simplified: $Mg_2(OH)PO_4$).[33] The title compound is accessible at an intermediate pH value of 5.0 in the lithium–cobalt–(hydrogen) phosphate system, whereas the high-voltage cathode material $LiCoPO_4$ and the cobalt hydroxide hydrogen phosphate $Co_3(OH)_2(PO_3OH)_2$ are formed under alkaline (pH = 8.0) and acidic ($3.0 \leq pH \leq 4.5$) conditions, respectively. We therefore started to discuss the structure of the title compound $Co_{11.0(1)}Li_{1.0(2)}[(OH)_5O][(PO_3OH)(PO_4)_5]$ first, before briefly investigating synthetic aspects and physical properties, including infrared and X-ray absorption spectroscopy, magnetic and thermal properties, in more detail.

EXPERIMENTAL SECTION

Hydrothermal Synthesis. $Co_{11.0(1)}Li_{1.0(2)}[(OH)_5O][(PO_3OH)(PO_4)_5]$ (or simplified: $Co_{1.84(2)}Li_{0.16(3)}(OH)PO_4$) crystals were prepared by hydrothermal synthesis using a Berghof digestec™ pressure digestion system equipped with 50 mL teflon-lined (TFM–PTFE) stainless steel pressure vessels (DAB-2), a heating block (DAH-412), and a programmable temperature control unit (BTC-3000; NiCrNi temperature probe). The starting materials $LiOH \cdot H_2O$ (Bernd Kraft, ≥ 99.0%), $Co(CH_3COO)_2 \cdot 4\ H_2O$ (Alfa Aesar, 98%), and $(NH_4)_2HPO_4$ (Merck EMSURE, ≥ 99.0%) were used in a Li:Co:P molar ratio of 2:1:1. First, 1.50 mmol $Co(CH_3COO)_2 \cdot H_2O$ and 1.50 mml $(NH_4)_2HPO_4$ were dissolved in 20 mL deionized water (high-purity water type I, Millipore, 18.2 MΩ·cm) to form a pink solution with pH = 5.5. A solution of 3.00 mmol $LiOH \cdot H_2O$ in 10 mL water was then added dropwise under continuous stirring. The pH of the resulting purple suspension (pH = 10) was adjusted to 5.0 using hydrochloric acid (Merck EMSURE, Ph. Eur., 37 wt%) with the help of indicator test strips (Merck MColorpHast™, pH range: 2.0–9.0, pH graduation: 0.5) in order to obtain a phase pure material. To investigate the influence of the pH value on the phase formation, the pH of the reaction mixture was varied in a range of 3.0–8.0, with an increment step of 0.5, by adjusting the amount of HCl added. The mixture was stirred vigorously, transferred to the teflon-lined pressure vessel, and sealed quickly. The temperature was ramped to 220 °C within 2 h and kept at that temperature for 20 h, followed by natural cooling after the reaction. The violet precipitate (*cf.* TOC graphic) was recovered from the suspension (pH = 5.0) by filtration, washed five times with 25 mL deionized water and 25 mL absolute ethanol (VWR AnalaR NORMAPUR, 99.95%), and then dried in air at 150 °C for 12 h.

Powder X-ray Diffraction (PXRD) and Rietveld Refinements. PXRD data were collected using a Stoe STADI P diffractometer (Mo $K_{\alpha 1}$ radiation, Ge(111) monochromator, λ = 0.70930 Å)

equipped with a Dectris MYTHEN DCS 1K silicon solid-state detector. The ground powders were sealed in borosilicate glass capillaries with a diameter of 0.5 mm (Hilgenberg), and then measured for 12 h in a 2θ range of 3–60° (PSD step: 0.015°; time/step: 30 s, three ranges). Silicon powder (a = 5.43088 Å) was used as external standard for the calibration of the patterns. Rietveld fitting was performed with the Jana2006 software[34] using the structure solution of the isostructural mineral satterlyite (simplified formula: $Fe_{1.54}Mg_{0.46}(OH)PO_4$; structure-chemical formula: $Fe_{9.24}Mg_{2.76}(OH,O)_6(PO_3OH)(PO_4)_5$, space group: $P31m$, ICSD no. 94842)[31] as a starting model. The background profile was fitted using a Chebyshev polynomial (35 coefficients), and peak asymmetry was corrected by the axial divergence model[35] embedded in Jana2006. An absorption correction[36] was applied using an estimated packing fraction of 0.6 for the capillary. The general atomic positions and isotropic thermal displacement parameters of the Co, P, and O atoms were refined without restraints, whereas all parameters of the H atoms were kept fixed. Furthermore, a Li substitution on both Co sites was assumed, while keeping the sum of the Li and Co site occupancy factors at 1. The positional atomic parameters were then standardized using the Structure Tidy routine[37] implemented in the Platon software package.[38] Finally, the Berar's factor[39] was applied to all refined parameters to obtain more realistic standard uncertainties.

Elemental Analysis. The Li content was analyzed by atomic absorption spectroscopy (AAS) using a Varian AA280FS sequential device. The Co and P amounts were measured by photometry on a Shimadzu UV-160 instrument. A Hekatech Euro EA CHNSO analyzer was used to determine the C, H, N, and S contents.

Soft X-ray Absorption Spectroscopy (XAS). Soft X-ray absorption spectroscopy (XAS) measurements were performed at beamline 8-2 of Stanford Synchrotron Radiation Laboratory (SSRL) using a 1100 mm^{-1} spherical grating monochromator (TGM) operated with 30 μm slits,

providing ~$2.0 \cdot 10^{10}$ ph·s^{-1} at 0.4 eV resolution in a 1 mm^2 beam spot as described in our previous work.[14] The powder sample was spread onto double-sided carbon tape and five scans of the Co $L_{2,3}$-edge μ(E) spectra were acquired under ultrahigh vacuum (10^{-9} Torr) at ambient temperature in the Auger electron yield (AEY; probing depth: ~2 nm), total electron yield (TEY; 2–5 nm), and fluorescence yield (FY; 50–100 nm) modes, respectively.[40] AEY was collected from a double-pass cylindrical mirror analyzer at a pass energy of 200 eV, TEY was observed through the drain current without bias, and FY was collected from a silicon diode (IRD AXUV-100) mounted at a higher glancing angle to reduce saturation effects. The spectra were normalized to the incoming flux and the energy scale aligned to meet the common energy scale of reference [41], followed by a linear background subtraction. The fitting, which was used to quantify the formal oxidation state of the Co ions, was limited to a small energy region across the L_3 edge (774–784 eV). In order to further experimentally evaluate the crystal field strength and symmetry, the experimental peak positions were extracted from the second derivatives.

Magnetic Measurements. DC magnetization measurements were performed using a Quantum Design MPMS XL7 SQUID (superconducting quantum interference device) magnetometer in the temperature range of T = 2–300 K under a magnetic field of up to 7 T. The powder sample was prepared using a calibrated gelatin capsule placed in a homogenous plastic straw. The temperature-dependence of the magnetic moment was measured in an applied magnetic field of 1 T after cooling the samples under a magnetic field of 7 T (field-cooled, FC) and 0 T (zero-field-cooled, ZFC). Magnetic hysteresis measurements were performed at magnetic field strengths between −7 T and 7 T at temperatures of 2 K, 10 K, 20 K, and 30 K, respectively.

Thermogravimetric Analysis (TGA) and Differential Scanning Calorimetry (DSC). The thermal stability was assessed by simultaneous TGA/DSC using a Mettler Toledo 1 STAR system.

An alumina crucible was filled with a specimen weight of approximately 5 mg and then heated up to 900 °C under an argon stream (10 mL·min^{-1}) at a heating rate of 10 °C·min^{-1}. Note that only the heating cycle could be monitored due to the simultaneous instrument setup.

RESULTS AND DISCUSSION

Powder X-ray Diffraction and Rietveld Refinement

Fig. 1 shows the Rietveld fit of the as-prepared title compound $Co_{11.1(1)}Li_{0.9(1)}[(OH)_5O][(PO_3OH)(PO_4)_5]$ (simplified formula for better comparability with the adamite- (*Pnnm*)[19] and caminite-type ($I4_1/amd$)[20] $Co_2(OH)PO_4$ phases: $Co_{1.85(1)}Li_{0.15(1)}(OH)PO_4$), which was obtained from the hydrothermal process at pH = 5.0. According to scanning electron microscopy (SEM) (see inset of Fig. 1), the violet powder (*cf.* TOC graphic) consists of uniform crystals (~15 μm × 30 μm) with a unique elongated triangular pyramid morphology and a lamellar fine structure (for further details on the SEM analysis, please refer to the Supporting Information, section 2, and Fig. S2). The PXRD pattern (see Fig. 1 and Fig. S1) is in good agreement with the simulated patterns of the minerals satterlyite $Fe_{9.24}Mg_{2.76}(OH,O)_6(PO_3OH)(PO_4)_5$ (space group: $P31m$, $Z = 1$; ICSD no. 94842,[31] simplified: $Fe_{1.54}Mg_{0.46}(OH)PO_4$) and holtedahlite ($Mg_{12}(OH,O)_6(PO_3OH)(PO_4)_5$ ($P31m$, $Z = 1$; ICSD no. 64769,[33] simplified: $Mg_2(OH)PO_4$), suggesting that the phases are isostructural. In fact, all reflections can be fitted to the trigonal structure model of satterlyite[31] with good reliability factors (R_p = 4.04%, R_{wp} = 5.93%, χ^2 = 1.91; *cf.* Table 1; for atomic coordinates, thermal displacements parameters, and selected interatomic distances see Tables S7a and S8a). The unit cell volume of 547.70(3) Å^3 lies between the Fe (V = 562.71(9) Å^3)[31] and Mg (V = 539.3(3) Å^3)[33] counterparts (for a detailed comparison of the crystallographic data please refer to Table S1), which is in agreement with the trend of ionic radii

(with coordination number CN = 6) of Fe^{2+} (high-spin (HS): 0.78 Å), Co^{2+} (HS: 0.745 Å), and Mg^{2+} (0.72 Å) [42] as well as the observed shifts in the PXRD patterns (Fig. S1).

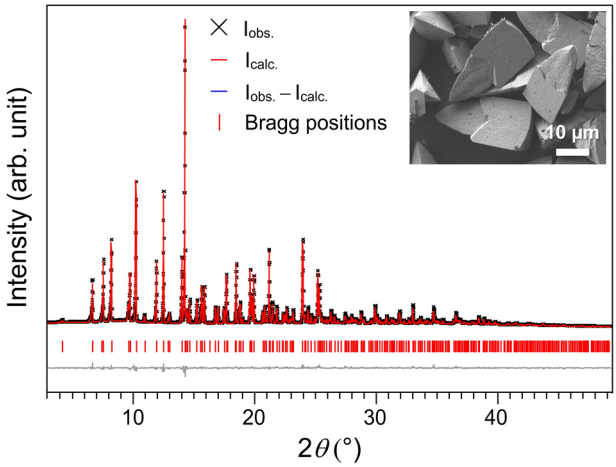

Figure 1. Rietveld fit of the powder X-ray diffraction data (Mo $K_{\alpha 1}$ radiation, 0.5 mm capillary, measurement time: 12 h) of $Co_{1.85(1)}Li_{0.15(1)}(OH)PO_4$ (crystal-chemical formula: $Co_{11.1(1)}Li_{0.9(1)}[(OH)_5O][(PO_3OH)(PO_4)_5]$, space group: $P31m$, $Z = 1$) prepared by the hydrothermal process at pH = 5.0. Inset: Scanning electron microscopy image demonstrating that the sample consists of uniform, well-dispersed crystals with an elongated triangular pyramid morphology and dimensions of ~15 µm × 30 µm.

Since the results of the elemental analysis suggested the presence of significant amounts of lithium in the material (see later in the discussion and Table 2), a partial substitution of the Co sites with Li was tentatively refined. The refinement resulted in statistically significant Li occupancies of 2.9(8)% on the Co1 site, and 12.2(8)% for the Co2 position. Mixed site occupation has also been reported for satterlyite, but with the divalent cation Mg^{2+}.[31] Although the Li population on the Co1 site is rather low and hard to determine with X-rays, we concluded that Li–Co mixing appears on both sites because further studies showed that both sites show significant mixing for

Table 1. Crystallographic Parameters of $Co_{1.85(1)}Li_{0.15(1)}(OH)PO_4$ as Refined from Powder X-ray Diffraction Data (T = 298 K) [a]

Simplified formula	**$Co_{1.85(1)}Li_{0.15(1)}(OH)PO_4$**
Crystal-chemical formula	$Co_{11.1(1)}Li_{0.9(1)}[(OH)_5O][(PO_3OH)(PO_4)_5]$
M_r (g·mol^{-1})	1333.3
Space group (no.)	$P31m$ (157)
Z	1
a (Å)	11.2533(4)
c (Å)	4.9940(2)
V (Å^3)	547.70(3)
F(000)	645
ρ (calcd.) (g·cm^{-3})	4.038(1)
R_p	0.0404
R_{wp}	0.0593
R_{exp}	0.0326
R_F	0.0474
R_B	0.0647
χ^2	1.91
Data/restraints/parameters	3803/0/91

[a] The standard deviations (in parentheses) were corrected using the Berar's factor.

the solid solutions with the general composition $Co_{2-x}Li_x(OH)PO_4$ at overall higher Li contents x (see later in the text and Fig. S7). Moreover, the free refinement of the Co occupancy factors (without Li substitution) indicated that both Co sites are not completely filled (occupancies: 97.3(7)% on Co1 and 88.1(7)% on Co2). These Co populations are comparable to the results of the Li/Co mixed model (occupancies: 97.1(8)% Co : 2.9(8)% Li on Co1/Li1 (≡ M1) and 87.8(8)%

Co : 12.2(8)% Li on Co2/Li2 (≡ *M*2); see Table S7a). The crystal-chemical formula $Co_{11.1(1)}Li_{0.9(1)}[(OH)_5O][(PO_3OH)(PO_4)_5]$ ($Z = 1$; corresponding to a simplified bulk composition of $Co_{1.85(1)}Li_{0.15(1)}(OH)PO_4$) is in good agreement with the composition derived from elemental analysis ($Co_{1.84(2)}Li_{0.16(3)}(OH)PO_4$, *cf.* Table 2) and the molar Co:P:O ratio of 1.87(6):1.00(2):5.0(1) derived from EDS (energy-dispersive X-ray spectroscopy) analysis (*cf.* Fig. S2). Note that this composition would not be charge-balanced assuming that the structure contains only divalent Co^{2+} ions. However, X-ray absorption experiments discussed later reveal that the deficit in positive electric charge due to the substitution by monovalent Li^+ ions is compensated by a corresponding amount of trivalent Co^{3+} in the framework.

The proton positions could not be refined from the X-ray data due to the low atomic scattering factor of H, but the infrared (IR) spectrum (*cf.* Fig. S5) revealed the presence of three independent hydroxyl groups, which is consistent with the literature.[32, 43] The proton distribution in satterlyite and holtedahlite has been a subject of thorough discussions in the literature.[31, 33, 43] Whereas the H1 and H2 positions, which are bonded to O ligands of [MO_6] octahedra (see structure discussion) could be localized, the position of H3, which belongs to a hydrogen phosphate [$PO_3(OH)$] unit, is strongly disordered in both structures and was not detectable in synthetic holtedahlite.[33] Although there are seven possible proton positions in the structure (3 × H1, 3 × H2, and 1 × H1, *cf.* Table S7a), the CHNS analysis of our compound (*cf.* Table 2) indicated that the asymmetric unit contains only six protons. This is in agreement with the findings for the Mg and Fe counterparts,[31, 33, 43] which suggest that the H sites are only partially occupied and the protons are distributed among the three hydroxyl groups. Assuming that the Co-containing phase also exhibits a disordered proton distribution, the correct crystal-chemical formula would therefore be $Co_{11.1(1)}Li_{0.9(1)}[(OH)_{6-x}O_x][(PO_4)_{1-x}(PO_3OH)_x](PO_4)_5$ (with $Z = 1$) because P3, which belongs to

the hydrogen phosphate group, has the multiplicity × 1 (*cf.* Table S7a). Hence, the compound does not represent a polymorph of $Co_2(OH)PO_4$ in the strict sense, although the deviation from the ideal composition is small. A theoretical end-member without a hydrogen phosphate unit (*i.e.*, $x = 0$) would be $Co_{11.1(1)}Li_{0.9(1)}(OH)_6(PO_4)(PO_4)_5$, which is equivalent to $6 \times [Co_{1.85(1)}Li_{0.15(1)}(OH)PO_4]$. However, this configuration seems to be unlikely since we could distinguish three hydroxyl bands in the infrared spectrum, one of which is related with the $[PO_3(OH)]$ group (for a detailed discussion of the IR spectrum, please refer to the Supporting Information, section 3 and Fig. S5).

Crystal Structure

The structure of $Co_{11.1(1)}Li_{0.9(1)}[(OH)_5O][(PO_3OH)(PO_4)_5]$ features octahedral $[MO_6]$ (M = Co, Li) and tetrahedral $[PO_4]$ building units that are connected to form a three-dimensional network. The M positions are characterized by two crystallographically independent Co sites that are partially substituted with Li. With 12.2(8)% Li, the $M2$ site is found to be richer in Li content than $M1$, which is substituted by 2.9(8)% Li (*cf.* Table S7a). The corresponding $[(M1)O_6]$ and $[(M2)O_6]$ octahedra are distorted and show $M1$–O distances in the range of 1.94(3)–2.25(3) Å (d_{av} = 2.11 Å), and $M2$–O distances of 2.10(2)–2.319(15) Å (d_{av} = 2.19 Å). The fact that the average M–O distances in the $[(M2)O_6]$ units, which are more highly substituted with Li, are slightly larger than in $[(M1)O_6]$ is consistent with the larger ionic radius of Li^+ compared to Co^{2+} (Li^+: 0.76 Å; Co^{2+} (HS): 0.745 Å).[42] However, taking into account the finite amount of Co^{3+} in the structure (see XAS discussion) and assuming that Li^+ and Co^{3+} are occupying the same M sites to form charge-balanced $[MO_6]$ octahedra, a contraction of the $M2$–O bond distance would be expected because of the significantly smaller ionic radius of Co^{3+} (HS: 0.61 Å).[42] Therefore, although it is not possible to derive the $Li^+/Co^{2+}/Co^{3+}$ ordering in the structure without further experiments, it is

likely that due to energetic reasons and similar to other compounds,[44] the Co^{3+} ions preferably reside on the *M*1 sites whereas the Li^{+} ions reside on the *M*2 sites, which would be consistent with the *M*1–O and *M*2–O distances.

The three P positions are represented by three unique, distorted [PO_4] tetrahedra with average P–O distances of 1.52 Å (P1–O), 1.58 Å (P2–O), and 1.54 Å (P3–O). Each of these units is distorted, and one longer and three shorter bonds are observed (*cf.* Table S8a). The P3 tetrahedron is further characterized by a hydroxyl group (O9–H3), giving rise to [PO_3(OH)] hydrogen phosphate units, with the proton H3 being strongly disordered, as discussed earlier.

The [(*M*1)O_6] and [(*M*2)O_6] octahedra are condensed via shared faces (*M*1: O3, O4, O5; *M*2: O4, O5, O6; *cf.* Fig. 2a), forming *M*1–*M*1 respective *M*2–*M*2 pairs with $d(M1–M1) = 2.815(6)$ Å and $d(M2–M2) = 2.860(8)$ Å. Interestingly, the resulting dimer units [$(M1)_2O_8$(OH)] and [$(M2)_2O_8$(OH)] feature *cis*-configured μ_2-bridging hydroxyl groups (O4–H1 and O5–H2), which has been confirmed by infrared spectroscopy (*cf.* Fig. S5). Note that although the calculation of O–H distances is not reliable using powder X-ray diffraction, the IR spectrum qualitatively confirms the presence of different force constants and hence, bond lengths.

The [$(M1)_2O_8$(OH)] and [$(M2)_2O_8$(OH)] dimers of face-sharing [MO_6] octahedra are further linked by shared edges (O1–O4 and O2–O5) to form alternating double strands which run parallel to the [001] direction and represent the dominant feature of the structure (Fig. 2b–d). As indicated in Fig. 2e, each double chain shares corners with six further double chains, reflecting the trigonal symmetry of the structure. The three independent [PO_4] tetrahedra are located in the channels of the resulting three-dimensional framework that run along [001]. Whereas the [(P1)O_4] and [(P2)O_4] units are linked *via* all four corners, the [(P3)O_3(OH)] group shares only three apical O atoms with the network.

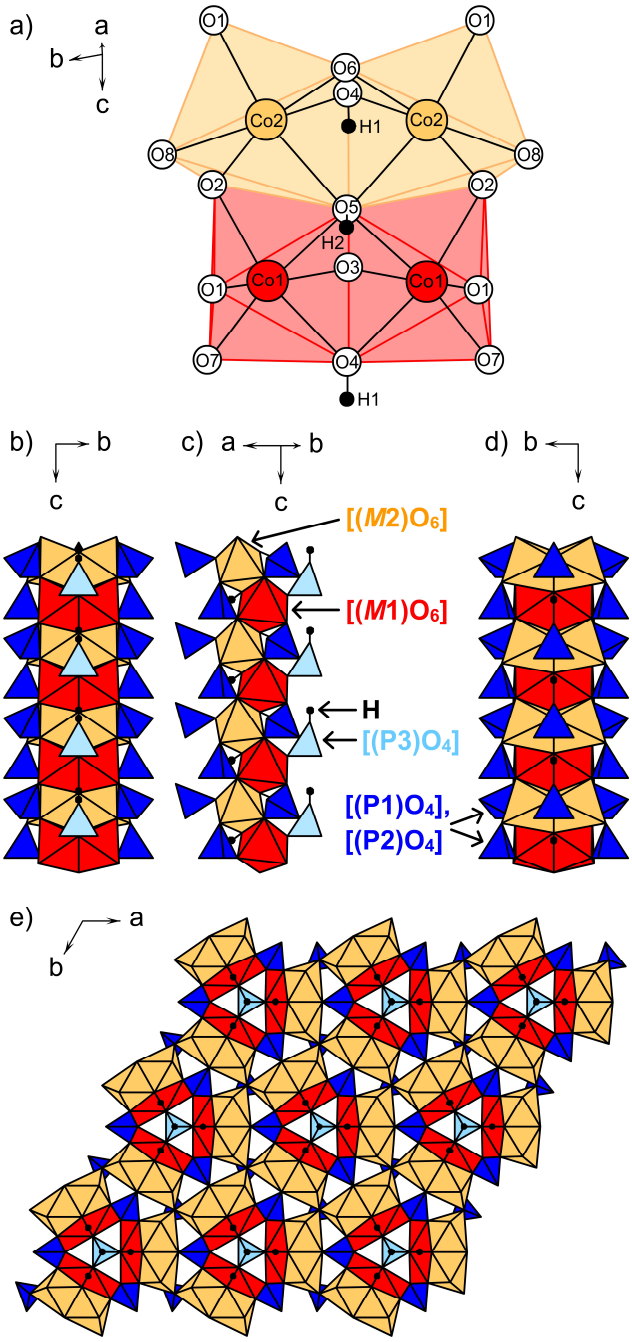

Figure 2. Polyhedral representation of the crystal structure of $Co_{11.1(1)}Li_{0.9(1)}[(OH)_5O][(PO_3OH)(PO_4)_5]$ (space group: $P31m$, $Z = 1$; simplified formula: $Co_{1.85(1)}Li_{0.15(1)}(OH)PO_4$). (a) The structure features two independent M (M = Co, Li) sites, $M1$ (red; populations: 97.1(8)% Co, 2.9(8)% Li) and $M2$ (orange; 87.8(8)% Co, 12.2(8)% Li), which are coordinated by O atoms (white) in an octahedral geometry. The $[(M1)O_6]$ (red) and $[(M2)O_6]$

(orange) units form face-sharing [(M1)$_2$O$_8$(OH)] and [(M2)$_2$O$_8$(OH)] dimers with μ_2-bridging OH groups (H: black; occupancy: 83.3%). (b–d) Through edge-sharing of the dimers along [001], alternating double chains are formed (viewed along different directions), which represent the dominant structural motif. (e) The double chains are further connected by three different, tetrahedral [PO$_4$] units to form a three-dimensional network in which each double chain shares corners with six other double chains. Whereas the [(P1)O$_4$] and [(P2)O$_4$] tetrahedra (dark blue) share all apical O atoms with the network, the [(P3)O$_3$(OH)] group (light blue) only contributes three O atoms.

Elemental Analysis

Table 2 compares the results of the elemental analysis of the XRD-pure sample with the theoretically expected values of a Li-free $Co_2(OH)PO_4$ material as well as the expected values based on the refined composition $Co_{1.85(1)}Li_{0.15(1)}(OH)PO_4$ from the PXRD data. The CHNS analysis indicates that the sample does not contain any detectable amounts of nitrogen or carbon, which might be present due to residues or decomposition products of the $(NH_4)_2HPO_4$ and $Co(CH_3COO)_2 \cdot 4\ H_2O$ precursors. This demonstrates that the washing step is sufficient to remove any side products formed in the synthesis. In contrast, 0.5(3) wt% H are found, which can be correlated to the hydroxyl groups in the structure as demonstrated by IR spectroscopy (see later in the discussion). Entrapped water as a possible source for hydrogen can be clearly ruled out because no water absorption bands are observed in the IR spectrum (*cf*. Fig. S5).

Table 2. Elemental Composition of (c) the As-Synthesized Material at pH = 5.0 in Comparison with the Theoretically Expected Values for (a) a Li-Free $Co_2(OH)PO_4$-Type Phase and (b) the Composition Derived from X-ray Diffraction [a,b]

Element	**a) Theoretical (Li-free phase)**	**b) Theoretical (expected from XRD)** [c]	**c) Measured**
H (wt%)	0.4	0.5	0.5(3)
Co (wt%)	51.3	49.1(2)	49.0(5)
Li (wt%)	0	0.50(3)	0.5(1)
P (wt%)	13.5	13.9	14.0(3)
O(estd.) (wt%)	34.8	36.0	36(2) [d]
n(H):*n*(P)	1:1	1:1	0.99(7):1.00(2)
n(Co):*n*(P)	1:1	1.85(1):1	1.84(2):1.00(2)
n(Li):*n*(P)	0	0.15(1):1	0.16(3):1.00(2)
n(O):*n*(P)	5:1	5:1	5.0(3):1.00(2)
Empirical formula	$Co_2(OH)PO_4$	$Co_{1.85(1)}Li_{0.15(1)}(OH)PO_4$	$Co_{1.84(2)}Li_{0.16(3)}(OH)_{0.99(7)}PO_4$

[a] The molar composition was determined from the experimental results (in wt%) of the CHNS, AAS, and photometric analyses, which were normalized to the P content (standard deviations are provided in parentheses). [b] The C, N, and S values were below the detection limit (= 0). [c] Note that standard deviations are only provided for the Co and Li contents since all other atomic sites were assumed to be fully occupied in the structure determination, and hence, do not exhibit standard deviations (see also Table S7a). [d] The O content was estimated from the H, Co, Li, and P contents (in wt%) based on the assumption that the sum of these elements accounts for 100 wt%.

In comparison to the ideal composition of a Li-free $Co_2(OH)PO_4$ phase (Table 2a), which was suggested for the *Pnnm* and $I4_1/amd$ polymorphs,[23, 24] a considerable amount of Li (0.5(1) wt%; *i.e.* significant within three standard deviations) is found in the as-prepared $P31m$-type compound whereas the Co content shows a deficit of approximately 2.2 wt% (Table 2c). The corresponding Li:Co:P molar ratio of 0.16(3):1.84(2):1.00(2) suggests that Co (starting from two equivalents Co

in the idealized, Li-free composition $Co_2(OH)PO_4$) is partially substituted by Li, which agrees with the X-ray diffraction experiments (Table 2b). Taking into account the H and O contents, the empirical formula of the material on the basis of the elemental analysis is $Co_{1.84(2)}Li_{0.16(3)}(OH)PO_4$ (from this point on, this formula is used for the pure material synthesized at pH = 5.0 for simplicity).

Synthesis Parameters

In order to gain further insights into the phase formation of $Co_{1.84(2)}Li_{0.16(3)}(OH)PO_4$ (general formula with varying Li contents *x*: $Co_{2-x}Li_x(OH)PO_4$), the influence of reaction conditions on the hydrothermal process based on the precursor system $LiOH \cdot H_2O$ – $Co(CH_3COO)_2 \cdot 4\ H_2O$ – $(NH_4)_2HPO_4$ was systematically investigated. While the temperature and reaction time demonstrated only minor influences, with the formation of the metastable $Co_{2-x}Li_x(OH)PO_4$ being preferred at low temperatures and shorter reaction times due to kinetic reaction control (not shown), the synthesis proved to be extremely sensitive towards the pH value of the reaction mixture. Upon variation of the pH value in a range of 3.0–8.0 (increment step: 0.5), a variety of Co-phosphates other than $Co_{2-x}Li_x(OH)PO_4$, namely the phases $Co_3(OH)_2(PO_3OH)_2$ (space group: $P2_1/c$, ICSD no. 67489)[45] and olivine-type $LiCoPO_4$ (*Pnma*, ICSD no. 431999),[16] were obtained. For pH values ≤ 2.5, no precipitate was formed from the reaction, suggesting that all components remained dissolved under strongly acidic conditions. The refined phase fractions *versus* the pH value of the reaction mixture are shown in Fig. 3 (for the individual Rietveld fits and details on the refinements please refer to Fig. S6 and Tables S4–S10 in the Supporting Information). Under acidic conditions at 3.0 ≤ pH ≤ 4.5, the formation of phase pure $Co_3(OH)_2(PO_3OH)_2$ is favored, while $Co_{2-x}Li_x(OH)PO_4$ and $LiCoPO_4$ compete as reaction products at 5.5 ≤ pH ≤ 7.5. The pH at

which pure $Co_{2-x}Li_x(OH)PO_4$ (with $x = 0.15(1)$) is formed is restricted to a very narrow region around pH 5.0. At pH = 5.5, the synthesis already yields 6.8(7) wt% $LiCoPO_4$ as a side product. The $LiCoPO_4$ fraction rises strongly until a single-phase olivine material is obtained under alkaline conditions (pH = 8.0). At pH > 8.0, a mixture of $LiCoPO_4$ and $Co_{11}(OH)_6(HPO_3)_8$ (space group: $P6_3mc$, ICSD no. 72431)[46] was obtained (not shown).

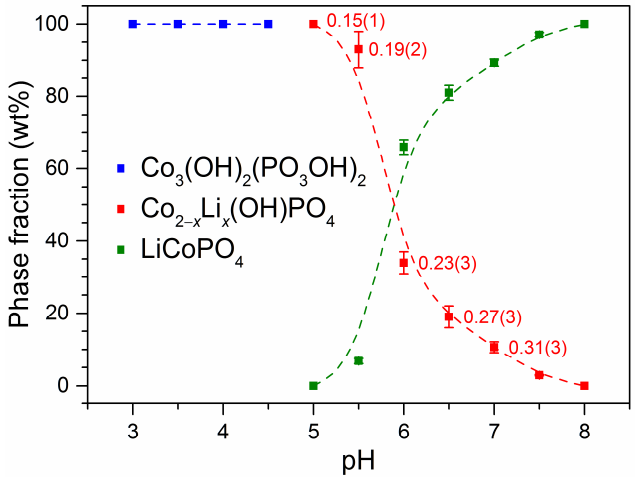

Figure 3. Phase fractions (in wt%; obtained from multi-component Rietveld refinements) *versus* pH value of the reaction mixture demonstrating that the formation of the phases $Co_3(OH)_2(PO_3OH)_2$ (space group: $P2_1/c$), $Co_{2-x}Li_x(OH)PO_4$ ($P31m$; the refined Li contents x are displayed in red along the data points for pH = 5.0–7.0 with standard deviations in parentheses), and $LiCoPO_4$ (*Pnma*) from the hydrothermal process is extremely pH-sensitive. It is evident that a pure $Co_{2-x}Li_x(OH)PO_4$-type material is only realized at pH = 5.0. Non-visible error bars are smaller than the data points. Data points not shown correspond to a phase fraction of 0 wt%, meaning that no reflections of the respective phases were detected in the PXRD pattern.

The observed variation in reaction products strongly reflects the pH sensitivity of the hydrothermal process. One interesting aspect is that the phases $Co_3(OH)_2(PO_3OH)_2$,

$Co_{2-x}Li_x(OH)PO_4$, and $LiCoPO_4$ involve phosphate groups with different degrees of protonation (HPO_4^{2-} → HPO_4^{2-}/PO_4^{3-} (*cf.* crystal structure) → PO_4^{3-}). This can be related to the dissociation equilibria of phosphoric acid:[47]

$$(1)\ H_3PO_4 \rightleftharpoons H_2PO_4^- + H^+,\ pK_{a1} = 2.16$$

$$(2)\ H_2PO_4^- \rightleftharpoons HPO_4^{2-} + H^+,\ pK_{a2} = 7.21$$

$$(3)\ HPO_4^{2-} \rightleftharpoons PO_4^{3-} + H^+,\ pK_{a3} = 12.32$$

According to the pK_a values, the predominant orthophosphate species in the pH range used for the hydrothermal synthesis (3.0–8.0) would be $H_2PO_4^-$ (dihydrogen phosphate) and HPO_4^{2-} (hydrogen phosphate). However, under hydrothermal synthesis conditions, which involve high temperature and pressure and the presence of various reactants, the equilibria seem to be shifted towards HPO_4^{2-} and PO_4^{3-}. In this context, it is also worth noting that the phase fractions of $Co_{2-x}Li_x(OH)PO_4$ and $LiCoPO_4$ *versus* pH in Fig. 3 follow a trend that resembles the phosphate equilibrium curves. This is consistent with the fact that similar trends with respect to the phase formation were observed when alternative phosphate sources (such as *e.g.* H_3PO_4 and $NH_4H_2PO_4$) were used as starting materials (not shown). Furthermore, the cobalt and hydroxide contents per formula unit decrease with increasing pH value (Co^{2+}: 3 → (2−*x*) → 1, OH^-: 2 → 1 → 0), while the Li contents increase (0 → *x* → 1). This agrees with a report by Huang and co-workers,[48] who suggested that the formation of phases such as $Co_3(OH)_2(PO_3OH)_2$ and $LiCoPO_4$ is the result of a dissolution–recrystallization process involving $Co(OH)_2$ as intermediate. The formation of Li-deficient phases in acidic media was related to the corrosion of the crystals and the solubility of LiOH under these conditions.

In agreement with this finding, the structure refinements reveal that the metal content and distribution in the individual phases is also affected by the pH value. In the case of

$Co_{2-x}Li_x(OH)PO_4$, the Li content x (and hence, the Co^{3+} content) almost linearly increases in a range of $0.15(1) \leq x \leq 0.31(3)$ with increasing pH value (Fig. 3 and Fig. S7a). There appears to be a preference for Li substitution on the *M*2 site for all compositions $Co_{2-x}Li_x(OH)PO_4$, although the Li occupancies on the *M*1 site increase more rapidly with higher pH (see Table S7, Fig. S7a). The cell volumes of $Co_{2-x}Li_x(OH)PO_4$ linearly decrease with increasing Li content x (Fig. S7b). According to the ionic radii (CN = 6) of Li^+ (0.76 Å) and Co^{3+} (HS: 0.61 Å), *versus* Co^{2+} (HS: 0.745 Å),[42] this decrease is mainly related to the concomitant increase of the Co^{3+} content, and hence, is in good agreement with what is expected for solid solutions according to Vegard's law.[49] Despite the fact that the refinement of Li contents is not very reliable by means of X-ray methods (*cf.* low atomic scattering factor of Li), this suggests that the phase displays a certain phase width. Therefore, future experiments should focus onto compositional tuning of $Co_{2-x}Li_x(OH)PO_4$ in order to identify the phase width and probably modify the material properties (*e.g.* by varying the stoichiometry of the precursors). It has to be pointed out that within the scope of our investigations, all attempts to prepare a Li-free *P*31*m*-$Co_2(OH)PO_4$ phase by using only $Co(CH_3COO)_2 \cdot 4\ H_2O$ and $(NH_4)_2HPO_4$ as precursors proved unsuccessful, resulting in single-phase $Co_3(OH)_2(PO_3OH)_2$ as the product (not shown). This suggests that the *P*31*m*-framework is probably stabilized by partial Li substitution (up to ~16 at%) as opposed to the lithium-free *Pnnm* and *I*4$_1$/*amd* $Co_2(OH)PO_4$ polymorphs. This would be in line with a report by Kolitsch *et al.*,[31] who suggested that a certain Mg content is necessary to stabilize the Fe homologue satterlyite. Whether a potential *P*31*m*-type $Co_2(OH)PO_4$ is experimentally accessible, should be further investigated by optimizing the synthesis parameters. On the other hand, the maximum Li content we found was $x = 0.31(3)$, which suggests that there is also an upper substitution limit above which the olivine structure

$LiCoPO_4$ (*Pnma*) is apparently more stable. This might be explained the presence of more Co^{3+} in the structure, which could intrinsically destabilize the metastable framework.

For $LiCoPO_4$, it was revealed that the phase is more prone to anti-site defects when prepared with increasing pH values, with the Co amount on the Li positions increasing (*cf.* Table S9). Since olivine-type $LiCoPO_4$ (*Pnma*) is a potential high-voltage cathode material for lithium-ion batteries,[8-10, 14-16] the investigation of the precursor system also provides valuable insights into this class of materials. The occurrence of anti-site defects results in a blocking of the Li-diffusion pathways, which reduces the electrochemical performance,[50] and hence suggests that the precursor system and the alkaline medium are not suitable for the production for high-performance cathode materials. The fact that $LiCoPO_4$ and $Co_{2-x}Li_x(OH)PO_4$ coexist over a wide pH range ($5.5 \leq pH \leq 7.5$) is furthermore highly relevant for the production of the material. In fact, we obtained $Co_{2-x}Li_x(OH)PO_4$ as a side phase with $LiCoPO_4$ using different solvothermal synthesis conditions especially when the pH value was not optimized. This is also in line with a report[51] on another polymorph of $LiCoPO_4$ (space group: $Pna2_1$), for which the orthorhombic *Pnnm*-type $Co_2(OH)PO_4$ polymorph was observed as a competing phase under non-ideal conditions. Interestingly, reflections originating from *P*31*m*-type $Co_{2-x}Li_x(OH)PO_4$ were also evident in PXRD patterns reported by other groups.[52] However, the peaks were correlated with other phases such as LiP_5, $Li_{0.62}CoO_2$, and CoO. For that matter, the investigations on $Co_{2-x}Li_x(OH)PO_4$ are highly significant for the wet-chemical synthesis of Co-containing cathode materials. Whether the homologue phases $M_{2-x}Li_x(OH)PO_4$ (M = Fe, Mn, Ni) exist and possibly also compete in the synthesis of the olivine-type cathode materials $LiMPO_4$ (M = Fe, Mn, Ni) is an interesting topic and should be investigated in consecutive studies.

X-ray Absorption Spectroscopy

In order to investigate the oxidation state of the Co ions in the structure, soft X-ray absorption spectroscopy on the $L_{2,3}$-edge was carried out, which is a powerful probe of the local electronic structure with sensitivity to symmetry, spin, valence, and covalency.[53, 54] Fig. 4 shows the normalized Co L_3-edge spectra of $Co_{1.84(2)}Li_{0.16(3)}(OH)PO_4$ compared to reference spectra of octahedrally coordinated (O_h, CN = 6) high-spin (HS) Co^{2+} (from CoO)[41] and HS Co^{3+} (from Sr_2CoO_3Cl)[55]. The $Co_{1.84(2)}Li_{0.16(3)}(OH)PO_4$ spectra are shown for both the TEY mode (Fig. 4b), probing about 2–5 nm deep, and the AEY mode (Fig. 4a), probing at the very top of the surface (~2 nm). Unfortunately, the more bulk-sensitive FY spectrum (~50–100 nm) was not of sufficient quality to be analyzed or discussed further and is therefore not shown.

It is clearly observed that the AEY (Fig. 4a) and TEY (Fig. 4b) spectra of $Co_{1.84(2)}Li_{0.16(3)}(OH)PO_4$ both show strong commonalities with the reference spectrum of O_h HS Co^{2+} (Fig. 4c) in shape and energy positions of the main features (in particular, the lowest energy peak or shoulder at 776.4 eV is characteristic of octahedrally coordinated Co^{2+}).[41] It can thus be discerned that high-spin divalent Co ions in an octahedral crystal field dominate the spectrum, which is in agreement with the crystal structure that features octahedral [MO_6] (M = Co, Li) units and the pink color of the powder (*cf.* TOC graphic). The minima of the second derivatives (*cf*. Fig. S8), which correspond to the experimental peak positions, reveal a small but significant shift in the peak positions of $Co_{1.84(2)}Li_{0.16(3)}(OH)PO_4$ (*i.e.* peak splitting) compared to the HS Co^{2+} reference which indicates an increased crystal field strength.[41] Moreover, the increase of spectral weight for both the AEY and TEY modes at higher energies, which is associated with Co^{3+} (*cf.* Fig. 4d) indicate the presence of Co^{3+}. This is in line with charge-balance arguments, which suggest that the $Co_{1.84(2)}Li_{0.16(3)}(OH)PO_4$ framework bears mixed-valent (+2/+3) Co ions due to the

substitution of the Co sites by Li^+ ions. Provided that the lack of positive charge caused by the Li^+ substitution (0.16 eq per formula unit) is compensated by the same amount of Co^{3+} ions (0.16 eq), the expected Co^{3+} content of would be ~8.7% (0.16/1.84; based on a total of 1.84 eq Co).

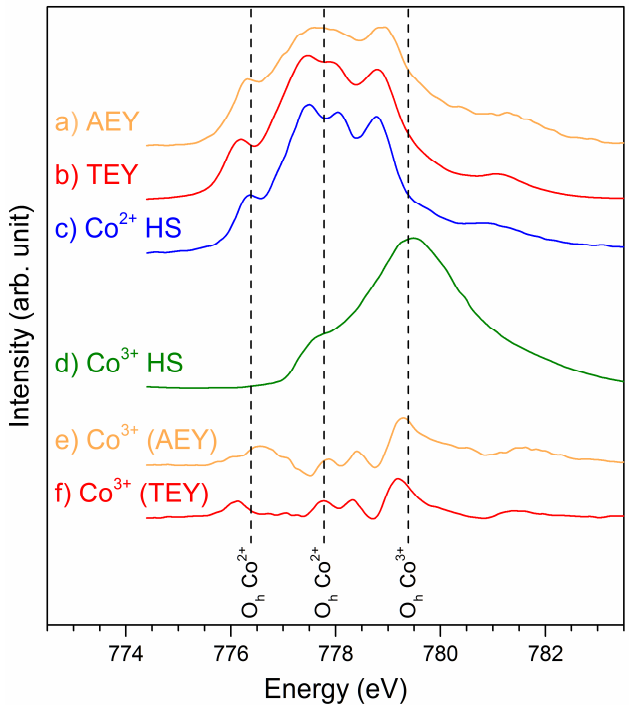

Figure 4. Normalized Co L_3-edge XAS spectra of $Co_{1.84(2)}Li_{0.16(3)}(OH)PO_4$ (prepared by hydrothermal synthesis at pH = 5.0) in the (a) AEY (orange) and (b) TEY (red) modes compared to reference spectra for octahedrally (O_h) coordinated (c) high-spin (HS) Co^{2+} (blue; CoO, adapted from ref. [41]), and (d) high-spin (HS) Co^{3+} (green; Sr_2CoO_3Cl, adapted from ref. [55]). (e) and (f) show the difference spectra resulting from the subtraction of 15% and 6% Co^{2+} from the AEY and TEY spectra of $Co_{1.84(2)}Li_{0.16(3)}(OH)PO_4$, respectively, which represents the Co^{3+} contributions. The increased Co^{3+} contribution at the top surface (AEY, *cf.* a,e) compared to the bulk (TEY; *cf.* b,f) of $Co_{1.84(2)}Li_{0.16(3)}(OH)PO_4$ is evident. All datasets have been aligned to match the common energy scale of reference [41]. The vertical dashed lines indicate the energies corresponding to O_h Co^{2+} (characteristic shoulder: 776.4 eV; doublet: 777.7 eV) as well O_h Co^{3+} (779.4 eV).

In order to extract the formal oxidation state, the AEY and TEY spectra were fitted with both high-spin Co^{2+} and Co^{3+} octahedral standards. The fitting of the TEY spectrum (*cf*. Fig. S9b) reveals an average Co^{3+} contribution of around (6.2 ± 2.0)%, which is close to the expected Co^{3+} content (~8.7 %), whereas a higher Co^{3+} content of about (14.6 ± 5.0)% was found for the most surface-sensitive AEY mode (*cf*. Fig. S9a). It can therefore be concluded that the top surface exhibits a higher Co^{3+} concentration than the bulk, which is also apparent from Fig. 4e,f, representing the individual Co^{3+} contributions that were obtained from subtraction of the fitted Co^{2+} contributions from the AEY and TEY spectra, respectively. This gradient in the Co^{3+} concentration might be explained by the formation mechanism. In order to obtain an electronically balanced, Li-bearing framework, part of the Co^{2+} ions are probably oxidized to Co^{3+} *in situ*, compensating for the lack of positive charge due to the Li^{+} substitution. It is likely that the oxidation preferably occurs on the particle surface since Co^{2+} is generally prone to oxidation in aqueous media. Therefore, it will be worth examining whether the Co oxidation (and Li substitution) can be hindered by using reducing agents such as glucose, ascorbic acid or hydrazine[14, 50] in the reaction mixture in order to produce a Li-free, Co^{2+}-only *P*31*m*-$Co_2(OH)PO_4$ framework.

Magnetic Properties

The magnetic properties of $Co_{1.84(2)}Li_{0.16(3)}(OH)PO_4$ are presented in Fig. 5. In the high temperature regime (T > 100 K), the magnetic susceptibility measured using a magnetic field of 1 T in field-cooled (FC) and zero-field-cooled (ZFC) conditions follow a Curie–Weiss law with a Weiss temperature of (−68 ± 2) K and an effective magnetic moment of (7.08 ± 0.05) μ_B (see Fig. S10). The negative Weiss temperature indicates that the dominant interaction between

neighboring magnetic ions is antiferromagnetic. This is in agreement with reports on the Li-free *Pnnm*- and $I4_1/amd$-type $Co_2(OH)PO_4$ polymorphs.[20, 23] The low-temperature behavior of the magnetic susceptibility, however, is different from that of the reported $Co_2(OH)PO_4$ phases. The first maximum of the magnetic susceptibility at around $T = 25$ K together with an almost linear magnetic field dependence of the magnetization at 10 K suggest the onset of a long-range antiferromagnetic order of $Co_{1.84(2)}Li_{0.16(3)}(OH)PO_4$ below 25 K. This temperature is close to the transition temperature of 20 K found in the tetragonal ($I4_1/amd$) modification of $Co_2(OH)PO_4$,[20] while it is much lower than the transition temperature of 71 K of the orthorhombic (*Pnnm*) $Co_2(OH)PO_4$ polymorph.[23] Furthermore, a second maximum of the ZFC magnetic susceptibility was found at around 9 K. Below this temperature, $Co_{1.84(2)}Li_{0.16(3)}(OH)PO_4$ exhibits a magnetic hysteresis with a finite remanent magnetization (see inset of Fig. 5 and Fig. S11), demonstrating the existence of a ferromagnetic component. However, no saturation of the magnetization is observed up to 7 T. This behavior is similar to that of *Pnnm*-$Co_2(OH)PO_4$ below 15 K,[23] indicating a spin-glass-like behavior with a blocking temperature of around 9 K. However, to further investigate this spin-glass-like behavior, AC-susceptibility measurements at different frequencies would be required. In total, the finite Li^+ and Co^{3+} concentrations in the $Co_2(OH)PO_4$ framework results in a reduction of the paramagnetic to antiferromagnetic transition as well as the blocking temperature of the spin-glass-like behavior. In order to unveil the structure-related magnetic details unambiguously, neutron diffraction measurements will be required.

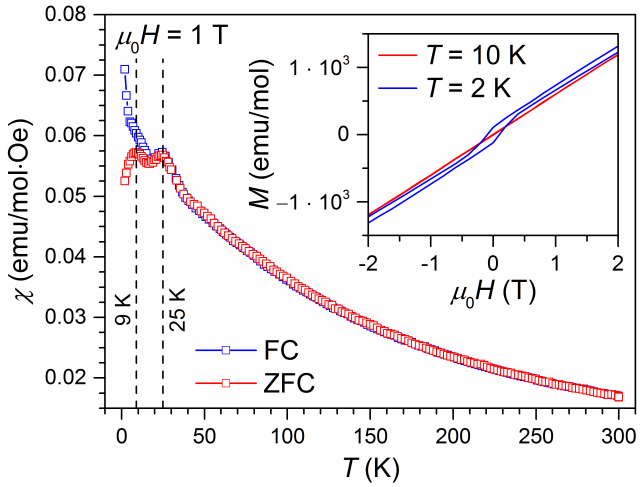

Figure 5. Magnetic susceptibility of $Co_{1.84(2)}Li_{0.16(3)}(OH)PO_4$ (prepared by hydrothermal synthesis at pH = 5.0) as a function of temperature measured at a magnetic field of 1 T under field-cooled (FC) and zero-field-cooled (ZFC) conditions. The vertical dashed lines indicate the temperature of the paramagnetic to antiferromagnetic transition (25 K) as well as the blocking temperature of the spin-glass-like behavior (9 K) at low temperature. Inset: Magnetic hysteresis curves measured at temperatures of T = 10 K and 2 K, respectively.

Thermal Stability

The thermal stability of $Co_{1.84(2)}Li_{0.16(3)}(OH)PO_4$ was investigated by TGA/DSC measurements, which demonstrate a metastable behavior of the material (Fig. 6a). Two signals are observed in the DSC curve, a small exothermic peak at 558 °C, and an endothermic peak at 663 °C. According to the TGA data, both transitions are accompanied by a weight loss that accounts for 4.6 wt% in total. The initial mass loss of about ~0.6 wt% starts around 440 °C, and is then followed by a distinct step of ~4.0 wt%. The fact that the weight loss onset occurs at rather high temperature implies that no residues of water or the cobalt acetate precursor are present (in agreement with the CHNS analysis, *cf.* Table 2), hence confirming the purity of the material.

According to the X-ray powder diffractogram of the dark violet post-TGA/DSC powder (Fig. 6b, for details on the Rietveld refinement refer to Tables S11–S17), a mixture containing 72.3(10) wt% CoO (space group: $Fm\bar{3}m$; ICSD no. 9865),[56] 15.1(5) wt% $Co_3(PO_4)_2$ ($P2_1/c$, ICSD no. 4268),[57] and 12.6(10) wt% olivine-type $LiCoPO_4$ (*Pnma*, ICSD no. 431999)[16] was formed upon heating. The formation of CoO and $Co_3(PO_4)_2$ upon decomposition is consistent with a report[19] on the *Pnnm* polymorph of $Co_2(OH)PO_4$, for which the same phases were observed (note that for the $I4_1/amd$ polymorph, no decomposition products were reported[20]). The occurrence of the additional Li-containing phase $LiCoPO_4$ provides further evidence for the partial Li-substitution of the $P31m$-type $Co_2(OH)PO_4$ framework.

Based on the TGA/DSC, *ex situ* PXRD as well as the XAS experiments, which demonstrated the presence of Co^{3+} in the structure, the decomposition process of $Co_{1.84(2)}Li_{0.16(3)}(OH)PO_4$ may be described according to Fig. 6c. Whereas the second mass loss step of 4.1 wt%, which is correlated with the endothermic signal around 663 °C, can most likely be attributed to the loss of water from the hydroxyl groups of the framework (*cf.* $[PO_3(OH)]$ and $[M_2O_8(OH)]$ units), the small initial weight loss of 0.6 wt% accompanying the exothermic peak around 558 °C may be the result of oxygen release. This step is driven by a redox reaction, in which the O^{2-} ions are oxidized to elemental O_2 (Eq. II) by the definite amount of Co^{3+} ions, which are in turn reduced to Co^{2+} (Eq. I). The sum of the expected weight losses from H_2O and O_2 is consistent with the experimental TGA mass loss of 4.6 wt% (*cf.* Fig. 6a). In total, the exothermic oxidation takes place first followed by the endothermic dehydration step. Furthermore, the estimated mass fractions of the crystalline decomposition products $Co_3(PO_4)_2$, CoO, and $LiCoPO_4$ in the solid residue after H_2O/O_2 release are equivalent to the refined values obtained from our multi-component Rietveld analysis (Fig. 6b) within one standard deviation, which further supports the suggested mechanism.

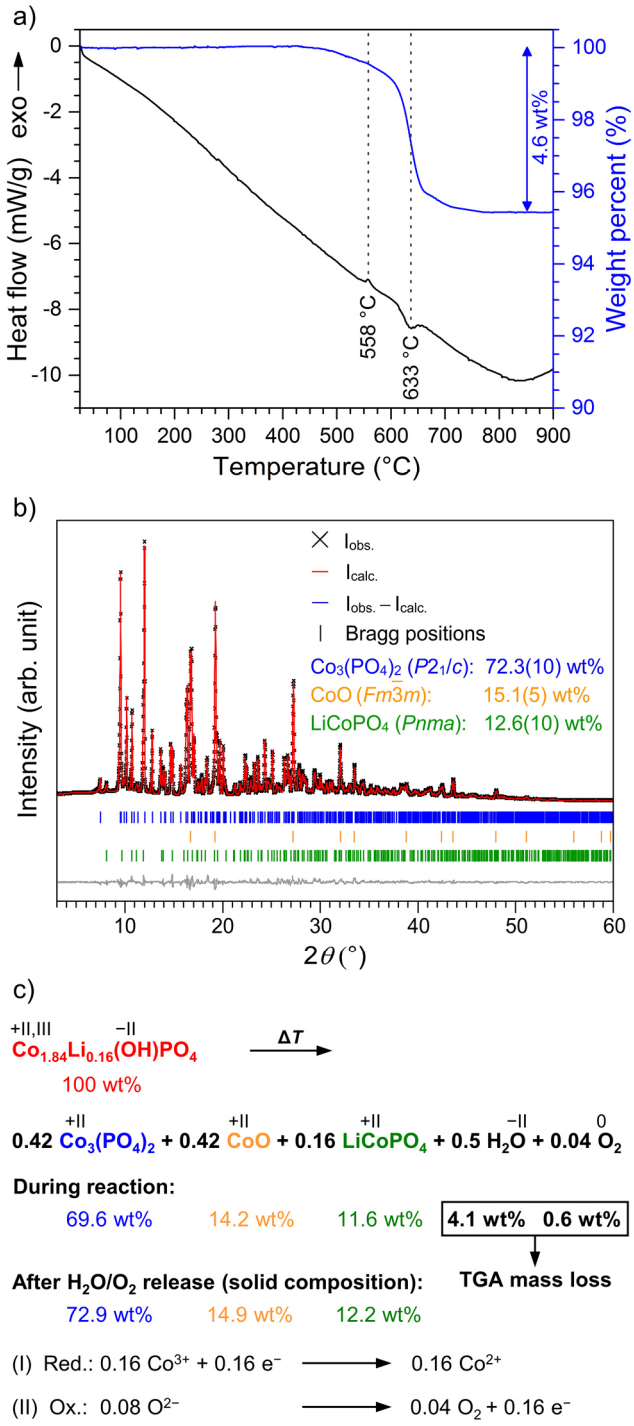

Figure 6. (a) DSC (black) and TGA (blue) curves of $Co_{1.84(2)}Li_{0.16(3)}(OH)PO_4$ measured under Ar in a temperature range of 30–900 °C (heating rate: 10 °C·min^{-1}). Two DSC signals are observed at 558 °C (exothermic) and 633 °C (endothermic), which are accompanied by a total weight loss

of 4.6 wt%. (b) Rietveld fit of the powder X-ray diffraction data (Mo $K_{\alpha1}$ radiation, 0.5 mm capillary, measurement time: 12 h) of the post TGA/DSC-material demonstrating that a mixture of crystalline CoO (space group: $Fm\bar{3}m$; ICSD no. 9865),[56] $Co_3(PO_4)_2$ ($P2_1/c$, ICSD no. 4268),[57] and olivine-type $LiCoPO_4$ (*Pnma*, ICSD no. 431999)[16] was formed upon heating. (c) Proposed thermal decomposition process and theoretically expected weight fractions (in wt%) of the involved phases. It can be inferred that the DSC signals and the weight loss observed in the TGA (a) are correlated with the release of water (dehydration) and oxygen (oxidation of oxide ions) as a result of a redox reaction.

CONCLUSION

A novel metastable, lithium-stabilized heterovalent cobalt (II,III) hydroxyl phosphate framework with the empirical formula $Co_{1.84(2)}Li_{0.16(3)}(OH)PO_4$ and the structure-chemical formula $Co_{11.0(1)}Li_{1.0(2)}[(OH)_5O][(PO_3OH)(PO_4)_5]$ was prepared by hydrothermal synthesis. The synthesis conditions, the crystal structure, and material properties were discussed.

The pH value was identified as a key parameter of the hydrothermal process, and the phase pure $Co_{2-x}Li_x(OH)PO_4$-type material is exclusively produced at an intermediate pH value of 5.0 ($x = 0.16(3)$). In contrast, $Co_3(OH)_2(PO_3OH)_2$ was formed in a more acidic medium ($3.0 \leq pH \leq 4.5$), whereas olivine-type $LiCoPO_4$ was obtained under alkaline conditions (pH = 8.0). The uniform crystals of the material exhibit a unique triangular pyramid morphology (dimensions: 15 µm × 30 µm) with a nanosheet-like primary structure. The trigonal phase (space group: $P31m$, a = 11.2533(4) Å, c = 4.9945(2) Å, V = 547.75(3) Å^3, Z = 1) is isostructural with natural phosphate minerals (satterlyite, holtedahlite) and features a partial Li substitution on the

Co sites. First experiments suggested that the Li substitution is crucial for the stabilization of the structure since the synthesis of a Li-free *P*31*m*-type $Co_2(OH)PO_4$ framework proved unsuccessful. The prevailing structural motif are double chains along the [001] direction, which are built from [M_2O_8(OH)] (*M* = Co, Li) dimers and interconnected by tetrahedral [PO_4] and [PO_3OH] groups. Whereas the occurrence of the OH groups was confirmed by infrared spectroscopy, X-ray absorption spectroscopy studies revealed that the framework features mixed-valent Co ions (+2/+3), the occurrence of Co^{3+} likely being the result of the Li^+ substitution in order to obtain a charge-balanced framework. Magnetic measurements demonstrated a paramagnetic to antiferromagnetic transition at $T = 25$ K and a spin-glass-like behavior with a blocking temperature of around 9 K. The metastable character of the mixed-valent framework was confirmed by thermogravimetric analysis and differential scanning calorimetry. Driven by a redox reaction and the intrinsic instability of Co^{3+}, the structure decomposes into CoO, $Co_3(PO_4)_2$, and $LiCoPO_4$ in a two-step process, with the oxidation of oxide ions to oxygen being the first (558 °C, exothermic) and the dehydration the second (633 °C, endothermic) step.

To conclude, this work provides fundamental insights into the synthesis and structure–property relationships of cobalt hydroxide framework structures, and hence paves the way into modifying the material properties for potential applications. Due to the occurrence of mixed-valent Co (II,III) ions in the hydroxide–hydrogen phosphate–phosphate framework, it may act as a good oxygen-evolving catalyst (OEC; *e.g.* for water splitting), similarly to the cobalt–phosphate (Co–Pi) catalyst.[5-7] As first experiments revealed that the solid solutions $Co_{2-x}Li_x(OH)PO_4$ (x = 0.15(1)–0.35(3); refined from X-ray data) can be prepared, with the Li content increasing with the pH value of the reaction mixture, future studies should focus onto compositional tuning of the material (*e.g.* by varying the stoichiometry of the starting materials), which might be of significance for its

possible application in catalytic processes. In that context, the destabilizing effect of Co^{3+} as well as the charge ordering of the $Li^{+}/Co^{2+}/Co^{3+}$ ions in the structure should be examined. Furthermore, the synthesis of a non-Li-containing, $Co_2(OH)PO_4$ *P*31*m*-type cobalt(II) framework should be pursued. In order to completely resolve the structure, the proton distribution has to be determined with respect to the H positions, degree of saturation, and a possible delocalization. Since the formation of $Co_{2-x}Li_x(OH)PO_4$ as a side product of the hydrothermal synthesis of the olivine-type cathode material $LiCoPO_4$ (*Pnma*) was revealed, it will be interesting to explore whether the isostructural homologues $M_{2-x}Li_x(OH)PO_4$ (*M* = Fe, Mn, Ni) exist and hence, also represent side products of the respective hydrothermal synthesis processes towards the cathode materials $LiMPO_4$ (*M* = Fe, Mn, Ni).

ASSOCIATED CONTENT. **Supporting Information**. The following material is available free of charge on the ACS Publications website at DOI: 10.1021/acs.inorg-chem.xxxxxxx: 1. Comparison of the PXRD pattern and lattice parameters with satterlyite and holtedahlite; 2. SEM and EDS; 3. IR spectrum; 4. Rietveld refinements of the PXRD patterns of the samples obtained from hydrothermal syntheses in a pH range of 3.0–8.0; 5. Additional XAS data; 6. Additional magnetic data; 7. Rietveld refinement of the PXRD pattern of the post-TGA/DSC material (PDF).

CCDC 1544992, 1544996–1545001, and 1545128–1545137 contain the supplementary crystallographic data for this paper. The data can be obtained free of charge from The Cambridge Crystallographic Data Centre via www.ccdc.cam.ac.uk/structures. Alternatively, the cif files may also be obtained from FIZ Karlsruhe, 76344 Eggenstein-Leopoldshafen, Germany (e-mail: crysdata@fiz-karlsruhe.de), on quoting the CSD numbers 432907–432923.

AUTHOR INFORMATION

Corresponding Authors

* E-mail: jennifer.ludwig@tum.de and tom.nilges@lrz tum.de, Tel.: +49 89 289 13110,

Fax: +49 89 289 13762

Author Contributions

J. L. conceived and designed this work, and carried out the synthesis, material characterization (PXRD, IR, SEM/EDS), and data analysis (under the supervision of M. M. D. and T. N.). S. G. and D. N. performed and analyzed magnetic and XAS measurements, respectively. J. L. wrote the manuscript. All the authors approved the final version of this manuscript.

Funding Sources

This work has been funded by the Fonds der Chemischen Industrie and the TUM Graduate School. The soft XAS experiments were performed at SSRL (Stanford Synchrotron Radiation Lightsource), a Directorate of SLAC National Accelerator Laboratory supported by the US Department of Energy, Office of Science, and Office of Basic Energy Sciences under contract number DE-AC02-76SF00515.

ACKNOWLEDGMENT

The authors would like to thank P. Madhikar for TGA/DSC measurements, and U. Ammari for elemental analysis. The help of C. Denk with a part of the syntheses is gratefully acknowledged. J. Ludwig thanks the Fonds der Chemischen Industrie and the TUM Graduate School for financial support of her Ph.D. project.

ABBREVIATIONS

AAS, atomic absorption spectroscopy; AC, alternating current; AEY, Auger electron yield; CN, coordination number; DC, direct current; DSC, differential scanning calorimetry; EDS, energy-dispersive X-ray spectroscopy; FC, field-cooled; IR, infrared; FY, fluorescence yield; HS, high-spin; HT, hydrothermal; ICSD, Inorganic Crystal Structure Database; OEC, oxygen-evolving catalyst; OER, oxygen evolution reaction; PSD, position-sensitive detector; PTFE, poly(tetrafluoroethylene); PXRD, powder X-ray diffraction; SEM, scanning electron microscope; SQUID, superconducting quantum interference device; TEY, total electron yield; TFM, perfluoro(propylvinylether)-modified PTFE; TGA, thermogravimetric analysis; XAS, X-ray absorption spectroscopy; ZFC, zero-field-cooled.

REFERENCES

(1) Maspoch, D.; Ruiz-Molina, D.; Veciana, J., Old materials with new tricks: multifunctional open-framework materials. *Chem. Soc. Rev.* **2007,** 36, (5), 770-818.

(2) Hogarth, C. A.; Jamel Basha, M., Electrical conduction in cobalt-phosphate glasses. *J. Phys. D* **1983,** 16, (5), 869-878.

(3) Anderson, M. T.; Phillips, M. L. F.; Sinclair, M. B.; Stucky, G. D., Synthesis of Transition-Metal-Doped $KTiOPO_4$ and Lanthanide-Doped $RbTiOAsO_4$ Isomorphs That Absorb Visible Light. *Chem. Mater.* **1996,** 8, (1), 248-256.

(4) Millet, J.-M. M., FePO catalysts for the selective oxidative dehydrogenation of isobutyric acid into methacrylic acid. *Catal. Rev. - Sci. Eng.* **1998,** 40, (1 & 2), 1-38.

(5) Kanan, M. W.; Nocera, D. G., In Situ Formation of an Oxygen-Evolving Catalyst in Neutral Water Containing Phosphate and Co^{2+}. *Science* **2008,** 321, (5892), 1072-1075.

(6) Kanan, M. W.; Surendranath, Y.; Nocera, D. G., Cobalt-phosphate oxygen-evolving compound. *Chem. Soc. Rev.* **2009,** 38, (1), 109-114.

(7) Zhong, D. K.; Gamelin, D. R., Photoelectrochemical Water Oxidation by Cobalt Catalyst ("Co-Pi")/α-Fe_2O_3 Composite Photoanodes: Oxygen Evolution and Resolution of a Kinetic Bottleneck. *J. Am. Chem. Soc.* **2010,** 132, (12), 4202-4207.

(8) Padhi, A. K.; Nanjundaswamy, K. S.; Goodenough, J. B., Phospho-olivines as Positive-Electrode Materials for Rechargeable Lithium Batteries. *J. Electrochem. Soc.* **1997,** 144, (4), 1188-1194.

(9) Amine, K.; Yasuda, H.; Yamachi, M., Olivine $LiCoPO_4$ as 4.8 V electrode material for lithium batteries. *Electrochem. Solid-State Lett.* **2000,** 3, (4), 178-179.

(10) Zaghib, K.; Guerfi, A.; Hovington, P.; Vijh, A.; Trudeau, M.; Mauger, A.; Goodenough, J. B.; Julien, C. M., Review and analysis of nanostructured olivine-based lithium recheargeable batteries: Status and trends. *J. Power Sources* **2013,** 232, 357-369.

(11) Masquelier, C.; Croguennec, L., Polyanionic (phosphates, silicates, sulfates) frameworks as electrode materials for rechargeable Li (or Na) batteries. *Chem. Rev.* **2013,** 113, (8), 6552-6591.

(12) Abrahams, S. C.; Bernstein, J. L., Crystal structure of paramagnetic ludlamite, $Fe_3(PO_4)_2.4H_2O$, at 298°K. *J. Chem. Phys.* **1966,** 44, (6), 2223-2229.

(13) Rabenau, A., The role of hydrothermal synthesis in preparative chemistry. *Angew. Chem.* **1985,** 97, (12), 1017-1032.

(14) Ludwig, J.; Marino, C.; Haering, D.; Stinner, C.; Nordlund, D.; Doeff, M. M.; Gasteiger, H. A.; Nilges, T., Facile, ethylene glycol-promoted microwave-assisted solvothermal synthesis of high-performance $LiCoPO_4$ as a high-voltage cathode material for lithium-ion batteries. *RSC Adv.* **2016,** 6, 82984-82994.

(15) Ludwig, J.; Haering, D.; Doeff, M. M.; Nilges, T., Particle size-controllable microwave-assisted solvothermal synthesis of the high-voltage cathode material $LiCoPO_4$ using water/ethylene glycol solvent blends. *Solid State Sci.* **2017,** 65, 100-109.

(16) Ludwig, J.; Marino, C.; Haering, D.; Stinner, C.; Gasteiger, H. A.; Nilges, T., Morphology-controlled microwave-assisted solvothermal synthesis of high-performance $LiCoPO_4$ as a high-voltage cathode material for Li-ion batteries. *J. Power Sources* **2017,** 342, 214-223.

(17) Rivera, J. P., The linear magnetoelectric effect in $LiCoPO_4$ revisited. *Ferroelectrics* **1994,** 161, (1-4), 147-164.

(18) Kharchenko, N. F.; Kharchenko, Y. N.; Szymczak, R.; Baran, M.; Schmid, H., Weak ferromagnetism in the antiferromagnetic magnetoelectric crystal $LiCoPO_4$. *Low Temp. Phys.* **2001,** 27, (9-10), 895-898.

(19) Harrison, W. T. A.; Vaughey, J. T.; Dussack, L. L.; Jacobson, A. J.; Martin, T. E.; Stucky, G. D., Two new adamite-type phases, $Co_2(OH)PO_4$ and $Zn_2(OH)PO_4$: structure-directing effect of organic additives. *J. Solid State Chem.* **1995,** 114, (1), 151-158.

(20) Wang, G.; Valldor, M.; Spielberg, E. T.; Mudring, A.-V., Ionothermal Synthesis, Crystal Structure, and Magnetic Study of Co_2PO_4OH Isostructural with Caminite. *Inorg. Chem.* **2014,** 53, (6), 3072-3077.

(21) Kokkoros, P., The structure of adamite. *Z. Kristallogr., Kristallgeom., Kristallphys., Kristallchem.* **1937,** 96, 417-434.

(22) Hill, R. J., The crystal structure and infrared properties of adamite. *Am. Mineral.* **1976,** 61, (9-10), 979-986.

(23) Rojo, J. M.; Mesa, J. L.; Lezama, L.; Pizarro, J. L.; Arriortua, M. I.; Fernandez, J. R.; Barberis, G. E.; Rojo, T., Spin-glass behavior in a three-dimensional antiferromagnet ordered

phase: Magnetic structure of $Co_2(OH)(PO_4)$. *Phys. Rev. B: Condens. Matter Mater. Phys.* **2002,** 66, (9), 094406/1-094406/13.

(24) de Pedro, I.; Rojo, J. M.; Jubera, V.; Fernandez, J. R.; Marcos, J. S.; Lezama, L.; Rojo, T., Effect of Ni^{2+} (S = 1) and Cu^{2+} (S = 1/2) substitution on the antiferromagnetic ordered phase $Co_2(OH)PO_4$ with spin glass behavior. *J. Mater. Chem.* **2004,** 14, (7), 1157-1163.

(25) de Pedro, I.; Jubera, V.; Rojo, J. M.; Lezama, L.; Sanchez Marcos, J.; Rodriguez Fernandez, J.; Mesa, J. L.; Rojo, T.; Arriortua, M. I., Magnetic properties of $Co_{2-x}Cu_x(OH)PO_4$ (x=0, 1 and 2). *J. Magn. Magn. Mater.* **2004,** 272-276, (Suppl. 1), E665-E666.

(26) de Pedro, I.; Rojo, J. M.; Lezama, L.; Rojo, T., Spectroscopic and magnetic properties of $Co_{1.7}Mn_{0.3}(OH)PO_4$. *Z. Anorg. Allg. Chem.* **2007,** 633, (11-12), 1847-1852.

(27) de Pedro, I.; Rojo, J. M.; Rodriguez Fernandez, J.; Lezama, L.; Rojo, T., Synthesis, Spectroscopic and Magnetic Properties of the $Co_2(OH)(PO_4)_{1-x}(AsO_4)_x$ [$0 \leq x \leq 1$] Solid Solution. *Eur. J. Inorg. Chem.* **2010**, (17), 2514-2522.

(28) Keefer, K. D.; Hochella, M. F., Jr.; De Jong, B. H. W. S., The structure of the magnesium hydroxide sulfate hydrate $MgSO_4 \cdot 1/3Mg(OH)_2 \cdot 1/3H_2O$. *Acta Crystallogr., Sect. B* **1981,** B37, (5), 1003-1006.

(29) Gheith, M. A., Lipscombite: a new synthetic "iron lazulite.". *Am. Mineral.* **1953,** 38, 612-628.

(30) Mandarino, J. A.; Sturman, B. D.; Corlett, M. I., Satterlyite, a new hydroxyl-bearing ferrous phosphate from the Big Fish River area, Yukon Territory [Canada]. *Can. Mineral.* **1978,** 16, (3), 411-413.

(31) Kolitsch, U.; Andrut, M.; Giester, G., Satterlyite, $(Fe,Mg)_{12}(PO_3OH)(PO_4)_5(OH,O)_6$: crystal structure and infrared absorption spectra. *Eur. J. Mineral.* **2002,** 14, (1), 127-133.

(32) Raade, G.; Mladeck, M. H., Holtedahlite, a new magnesium phosphate from Modum, Norway. *Lithos* **1979,** 12, (4), 283-287.

(33) Roemming, C.; Raade, G., The crystal structure of natural and synthetic holtedahlite. *Mineral. Petrol.* **1989,** 40, (2), 91-100.

(34) Petricek, V.; Dusek, M.; Palatinus, L., Crystallographic Computing System JANA2006: General features. *Z. Kristallogr. - Cryst. Mater.* **2014,** 229, (5), 345-352.

(35) Finger, L. W.; Cox, D. E.; Jephcoat, A. P., A correction for powder diffraction peak asymmetry due to axial divergence. *J. Appl. Crystallogr.* **1994,** 27, (6), 892-900.

(36) Cromer, D. T.; Liberman, D. A., Anomalous dispersion calculations near to and on the long-wavelength side of an absorption edge. *Acta Crystallogr., Sect. A* **1981,** A37, (2), 267-268.

(37) Gelato, L. M.; Parthe, E., STRUCTURE TIDY - a computer program to standardize crystal structure data. *J. Appl. Cryst.* **1987,** 20, (2), 139-143.

(38) Spek, A. L., Structure validation in chemical crystallography. *Acta Crystallogr., Sect. D: Biol. Crystallogr.* **2009,** 65, (2), 148-155.

(39) Berar, J. F.; Lelann, P., E.S.D.'s and estimated probable error obtained in Rietveld refinements with local correlations. *J. Appl. Crystallogr.* **1991,** 24, (1), 1-5.

(40) Lin, F.; Nordlund, D.; Markus, I. M.; Weng, T.-C.; Xin, H. L.; Doeff, M. M., Profiling the nanoscale gradient in stoichiometric layered cathode particles for lithium-ion batteries. *Energ. Environ. Sci.* **2014,** 7, (9), 3077-3085.

(41) Hibberd, A. M.; Doan, H. Q.; Glass, E. N.; de Groot, F. M. F.; Hill, C. L.; Cuk, T., Co Polyoxometalates and a Co_3O_4 Thin Film Investigated by L-Edge X-ray Absorption Spectroscopy. *J. Phys. Chem. C* **2015,** 119, (8), 4173-4179.

(42) Shannon, R. D., Revised effective ionic radii and systematic studies of interatomic distances in halides and chalcogenides. *Acta Crystallogr., Sect. A* **1976,** A32, (5), 751-767.

(43) Brunet, F.; Schaller, T., Protons in the magnesium phosphates phosphoellenbergerite and holtedahlite: an IR and NMR study. *Am. Mineral.* **1996,** 81, (3-4), 385-394.

(44) Strobridge, F. C.; Clement, R. J.; Leskes, M.; Middlemiss, D. S.; Borkiewicz, O. J.; Wiaderek, K. M.; Chapman, K. W.; Chupas, P. J.; Grey, C. P., Identifying the Structure of the Intermediate, $Li_{2/3}CoPO_4$, Formed during Electrochemical Cycling of $LiCoPO_4$. *Chem. Mater.* **2014,** 26, (21), 6193-6205.

(45) Effenberger, H., Structure refinement of tricobalt dihydroxide bis(hydrogen phosphate) and cobalt bis(dihydrogen phosphate) dihydrate. *Acta Crystallogr., Sect. C: Cryst. Struct. Commun.* **1992,** C48, (12), 2104-2107.

(46) Marcos, M. D.; Amoros, P.; Beltran-Porter, A.; Martinez-Manez, R.; Attfield, J. P., Novel crystalline microporous transition-metal phosphites $M_{11}(HPO_3)_8(OH)_6$ (M = Zn, Co, Ni). X-ray powder diffraction structure determination of the cobalt and nickel derivatives. *Chem. Mater.* **1993,** 5, (1), 121-128.

(47) Haynes, W. M., Dissociation Contants of Inorganic Acids and Bases In *CRC Handbook of Chemistry and Physics*, 94th ed.; CRC Press: Boca Raton, FL, 2013; pp 5-92.

(48) Huang, X.; Ma, J.; Wu, P.; Hu, Y.; Dai, J.; Zhu, Z.; Chen, H.; Wang, H., Hydrothermal synthesis of $LiCoPO_4$ cathode materials for rechargeable lithium-ion batteries. *Mater. Lett.* **2005,** 59, (5), 578-582.

(49) Vegard, L., Die Konstitution der Mischkristalle und die Raumfüllung der Atome. *Z. Physik* **1921,** 5, (1), 17-26.

(50) Chen, J.; Vacchio, M. J.; Wang, S.; Chernova, N.; Zavalij, P. Y.; Whittingham, M. S., The hydrothermal synthesis and characterization of olivines and related compounds for electrochemical applications. *Solid State Ion.* **2008,** 178, (31-32), 1676-1693.

(51) Jaehne, C.; Neef, C.; Koo, C.; Meyer, H.-P.; Klingeler, R., A new $LiCoPO_4$ polymorph via low temperature synthesis. *J. Mater. Chem. A* **2013,** 1, (8), 2856-2862.

(52) Wu, B.; Xu, H.; Mu, D.; Shi, L.; Jiang, B.; Gai, L.; Wang, L.; Liu, Q.; Ben, L.; Wu, F., Controlled solvothermal synthesis and electrochemical performance of $LiCoPO_4$ submicron single crystals as a cathode material for lithium ion batteries. *J. Power Sources* **2016,** 304, 181-188.

(53) de Groot, F. M. F.; Abbate, M.; van Elp, J.; Sawatzky, G. A.; Ma, Y. J.; Chen, C. T.; Sette, F., Oxygen 1s and cobalt 2p x-ray absorption of cobalt oxides. *J. Phys.: Condens. Matter* **1993,** 5, (14), 2277-2288.

(54) de Groot, F. M. F.; Fuggle, J. C.; Thole, B. T.; Sawatzky, G. A., The 2p x-ray absorption of 3d transition-metal compounds: an atomic multiplet description including the crystal field. *Phys. Rev. B: Condens. Matter* **1990,** 42, (9), 5459-5468.

(55) Hu, Z.; Wu, H.; Haverkort, M. W.; Hsieh, H. H.; Lin, H. J.; Lorenz, T.; Baier, J.; Reichl, A.; Bonn, I.; Felser, C.; Tanaka, A.; Chen, C. T.; Tjeng, L. H., Different Look at the Spin State of Co^{3+} Ions in a CoO_5 Pyramidal Coordination. *Phys. Rev. Lett.* **2004,** 92, (20), 207402/1-207402/4.

(56) Sasaki, S.; Fujino, K.; Takeuchi, Y., X-ray determination of electron-density distributions in oxides, magnesium oxide, manganese(II) oxide, cobalt oxide, and nickel(II) oxide, and atomic scattering factors of their constituent atoms. *Proc. Jpn. Acad., Ser. B* **1979,** 55, (2), 43-48.

(57) Anderson, J. B.; Kostiner, E.; Miller, M. C.; Rea, J. R., Crystal structure of cobalt orthophosphate $Co_3(PO_4)_2$. *J. Solid State Chem.* **1975,** 14, (4), 372-377.

For Table of Contents Only

SYNOPSIS. A new metastable compound, featuring a lithium-stabilized mixed-valent cobalt (II,III) hydroxide phosphate framework, $Co_{11.0(1)}Li_{1.0(2)}[(OH)_5O][(PO_3OH)(PO_4)_5]$ (space group: $P31m$, $Z = 1$, simplified composition: $Co_{1.84(2)}Li_{0.16(3)}(OH)PO_4$), was prepared by hydrothermal synthesis. The dominant structural feature are alternating double chains of $[M_2O_8(OH)]$ (M = Co, Li) dimer units, which run along the [001] direction and are connected via $[PO_4]$ and $[PO_3(OH)]$ tetrahedra. The synthesis conditions, crystal structure, and physical properties of the material are discussed.

TOC GRAPHIC

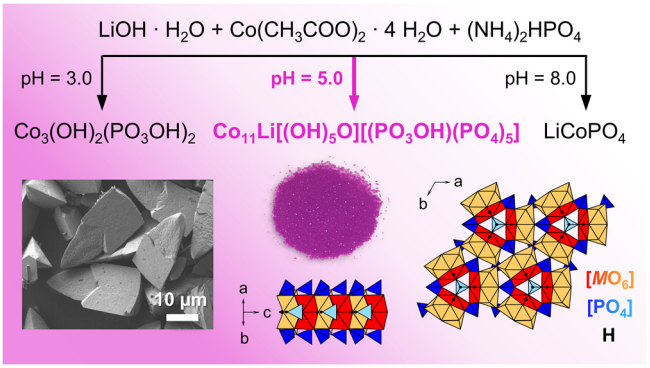

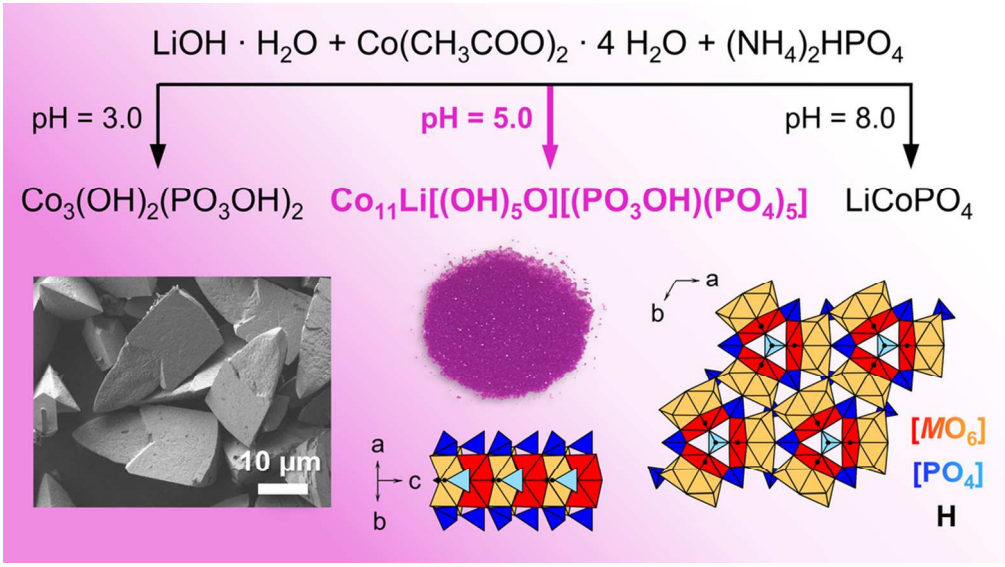

A new metastable compound, featuring a lithium-stabilized mixed-valent cobalt (II,III) hydroxide phosphate framework, $Co_{11.0(1)}Li_{1.0(2)}[(OH)_5O][(PO_3OH)(PO_4)_5]$ (space group: *P*31*m*, *Z* = 1, simplified composition: $Co_{1.84(2)}Li_{0.16(3)}(OH)PO_4$), was prepared by hydrothermal synthesis. The dominant structural feature are alternating double chains of $[M_2O_8(OH)]$ (*M* = Co, Li) dimer units, which run along the [001] direction and are connected via $[PO_4]$ and $[PO_3(OH)]$ tetrahedra. The synthesis conditions, crystal structure, and physical properties of the material are discussed.

47x26mm (600 x 600 DPI)

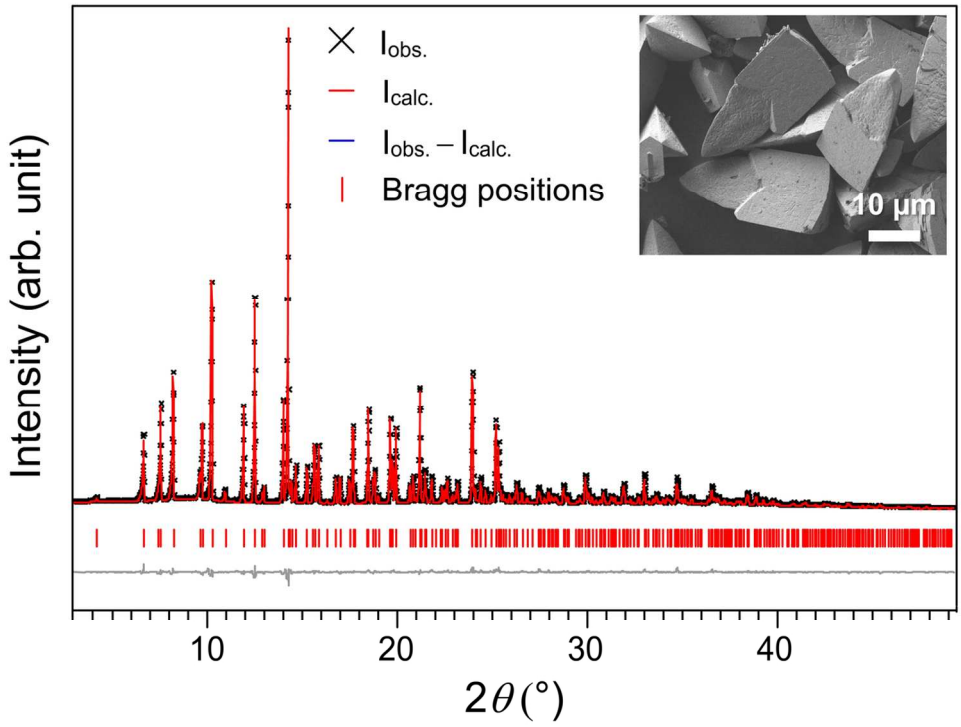

Figure 1. Rietveld fit of the powder X-ray diffraction data (Mo $K_{\alpha 1}$ radiation, 0.5 mm capillary, measurement time: 12 h) of $Co_{1.85(1)}Li_{0.15(1)}(OH)PO_4$ (crystal-chemical formula: $Co_{11.1(1)}Li_{0.9(1)}[(OH)_5O][(PO_3OH)(PO_4)_5]$, space group: *P*31*m*, *Z* = 1) prepared by the hydrothermal process at pH = 5.0. Inset: Scanning electron microscopy image demonstrating that the sample consists of uniform, well-dispersed crystals with an elongated triangular pyramid morphology and dimensions of ~15 μm × 30 μm.

63x47mm (600 x 600 DPI)

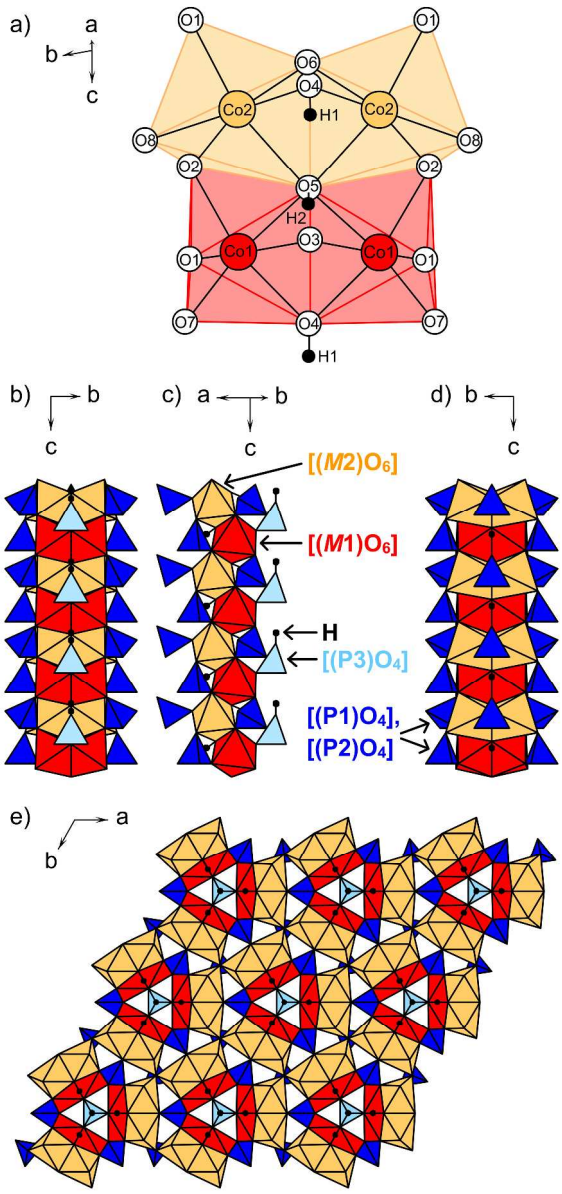

Figure 2. Polyhedral representation of the crystal structure of $Co_{11.1(1)}Li_{0.9(1)}[(OH)_5O][(PO_3OH)(PO_4)_5]$ (space group: $P31m$, $Z = 1$; simplified formula: $Co_{1.85(1)}Li_{0.15(1)}(OH)PO_4$). (a) The structure features two independent M (M = Co, Li) sites, $M1$ (red; populations: 97.1(8)% Co, 2.9(8)% Li) and $M2$ (orange; 87.8(8)% Co, 12.2(8)% Li), which are coordinated by O atoms (white) in an octahedral geometry. The $[(M1)O_6]$ (red) and $[(M2)O_6]$ (orange) units form face-sharing $[(M1)_2O_8(OH)]$ and $[(M2)_2O_8(OH)]$ dimers with μ_2-bridging OH groups (H: black; occupancy: 83.3%). (b–d) Through edge-sharing of the dimers along [001], alternating double chains are formed (viewed along different directions), which represent the dominant structural motif. (e) The double chains are further connected by three different, tetrahedral $[PO_4]$ units to form a three-dimensional network in which each double chain shares corners with six other double chains. Whereas the $[(P1)O_4]$ and $[(P2)O_4]$ tetrahedra (dark blue) share all apical O atoms with the network, the $[(P3)O_3(OH)]$ group (light blue) only contributes three O atoms.

178x376mm (600 x 600 DPI)

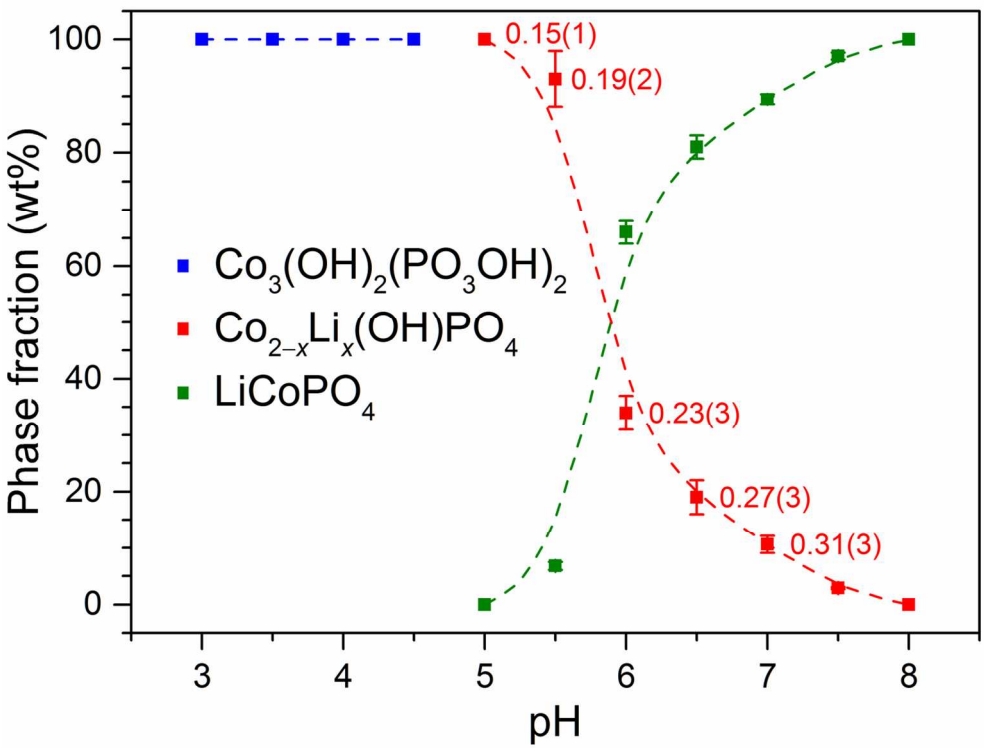

Figure 3. Phase fractions (in wt%; obtained from multi-component Rietveld refinements) versus pH value of the reaction mixture demonstrating that the formation of the phases $Co_3(OH)_2(PO_3OH)_2$ (space group: $P2_1/c$), $Co_{2-x}Li_x(OH)PO_4$ ($P31m$; the refined Li contents x are displayed in red along the data points for pH = 5.0–7.0 with standard deviations in parentheses), and $LiCoPO_4$ (*Pnma*) from the hydrothermal process is extremely pH-sensitive. It is evident that a pure $Co_{2-x}Li_x(OH)PO_4$-type material is only realized at pH = 5.0. Non-visible error bars are smaller than the data points. Data points not shown correspond to a phase fraction of 0 wt%, meaning that no reflections of the respective phases were detected in the PXRD pattern.

63x47mm (600 x 600 DPI)

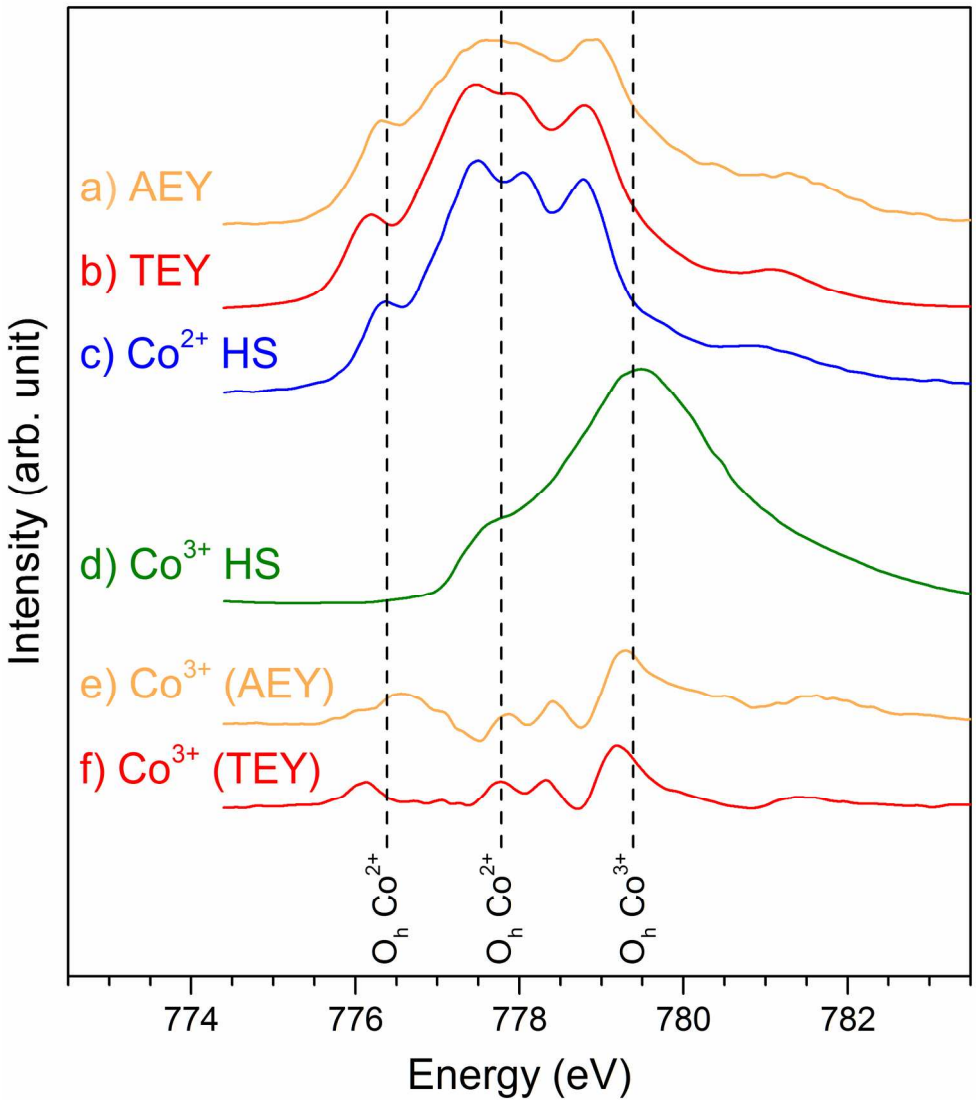

Figure 4. Normalized Co L_3-edge XAS spectra of $Co_{1.84(2)}Li_{0.16(3)}(OH)PO_4$ (prepared by hydrothermal synthesis at pH = 5.0) in the (a) AEY (orange) and (b) TEY (red) modes compared to reference spectra for octahedrally (O_h) coordinated (c) high-spin (HS) Co^{2+} (blue; CoO, adapted from ref. [45]), and (d) high-spin (HS) Co^{3+} (green; Sr_2CoO_3Cl, adapted from ref. [59]). (e) and (f) show the difference spectra resulting from the subtraction of 15% and 6% Co^{2+} from the AEY and TEY spectra of $Co_{1.84(2)}Li_{0.16(3)}(OH)PO_4$, respectively, which represents the Co^{3+} contributions. The increased Co^{3+} contribution at the top surface (AEY, *cf.* a,e) compared to the bulk (TEY; *cf.* b,f) of $Co_{1.84(2)}Li_{0.16(3)}(OH)PO_4$ is evident. All datasets have been aligned to match the common energy scale of reference [45]. The vertical dashed lines indicate the energies corresponding to O_h Co^{2+} (characteristic shoulder: 776.4 eV; doublet: 777.7 eV) as well O_h Co^{3+} (779.4 eV).

93x104mm (600 x 600 DPI)

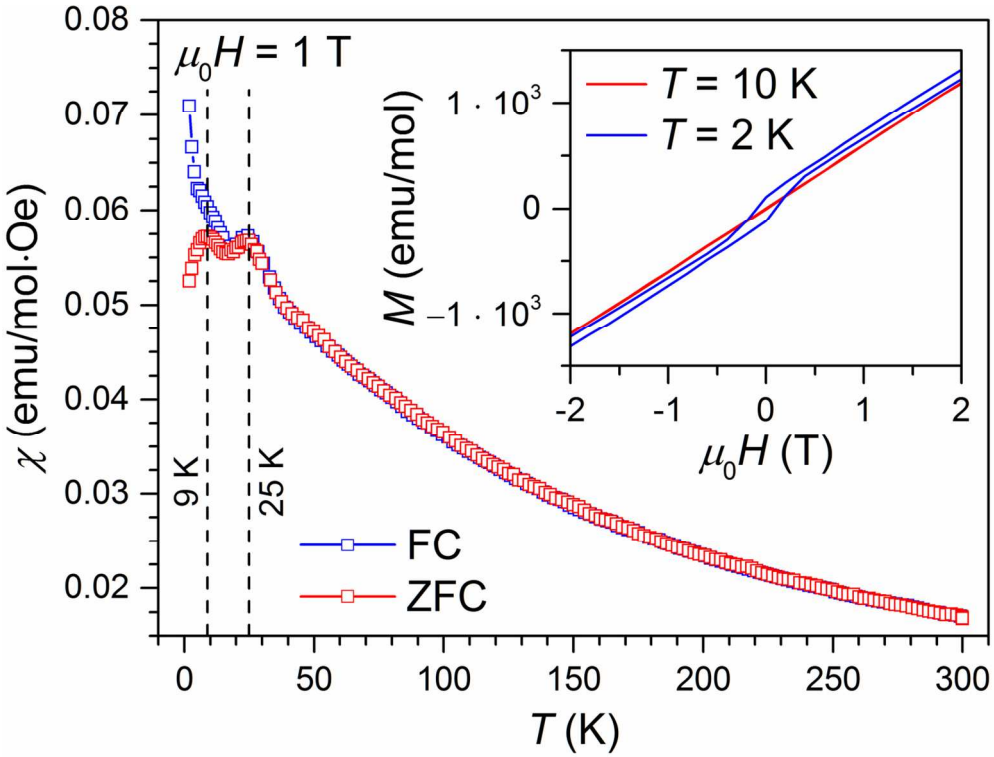

Figure 5. Magnetic susceptibility of $Co_{1.84(2)}Li_{0.16(3)}(OH)PO_4$ (prepared by hydrothermal synthesis at pH = 5.0) as a function of temperature measured at a magnetic field of 1 T under field-cooled (FC) and zero-field-cooled (ZFC) conditions. The vertical dashed lines indicate the temperature of the paramagnetic to antiferromagnetic transition (25 K) as well as the blocking temperature of the spin-glass-like behavior (9 K) at low temperature. Inset: Magnetic hysteresis curves measured at temperatures of T = 10 K and 2 K, respectively.

63x47mm (600 x 600 DPI)

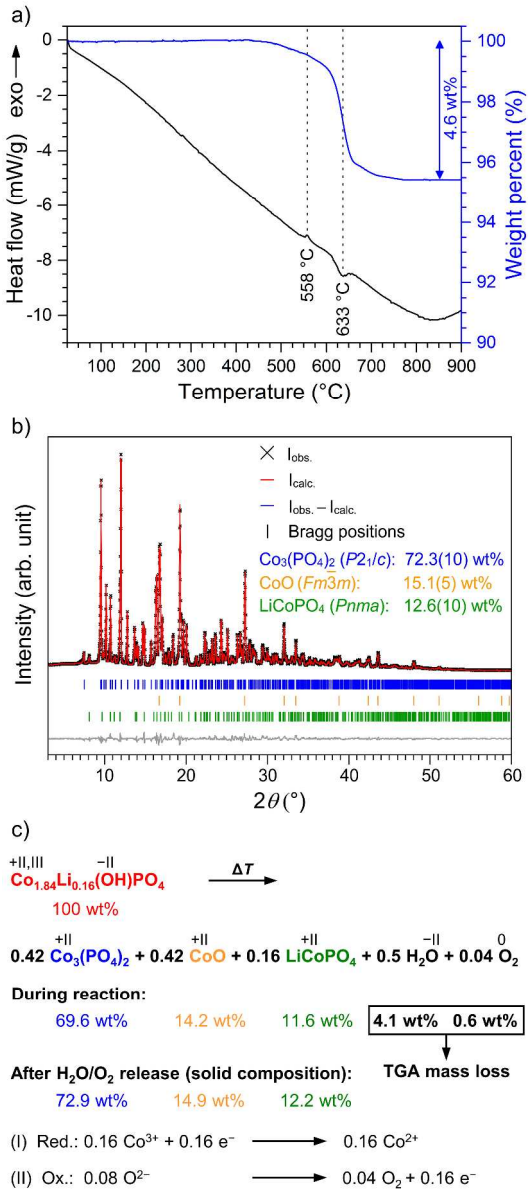

Figure 6. (a) DSC (black) and TGA (blue) curves of $Co_{1.84(2)}Li_{0.16(3)}(OH)PO_4$ measured under Ar in a temperature range of 30–900 °C (heating rate: 10 °C·min^{-1}). Two DSC signals are observed at 558 °C (exothermic) and 633 °C (endothermic), which are accompanied by a total weight loss of 4.6 wt%. (b) Rietveld fit of the powder X-ray diffraction data (Mo $K_{\alpha1}$ radiation, 0.5 mm capillary, measurement time: 12 h) of the post TGA/DSC-material demonstrating that a mixture of crystalline CoO (space group: *Fm*−3*m*; ICSD no. 9865),[64] $Co_3(PO_4)_2$ ($P2_1/c$, ICSD no. 4268),[65] and olivine-type $LiCoPO_4$ (*Pnma*, ICSD no. 431999)[19] was formed upon heating. (c) Proposed thermal decomposition process and theoretically expected weight fractions (in wt%) of the involved phases. It can be inferred that the DSC signals and the weight loss observed in the TGA (a) are correlated with the release of water (dehydration) and oxygen (oxidation of oxide ions) as a result of a redox reaction.

192x440mm (600 x 600 DPI)